inorganics

MDPI

Review

Review on Chemistry of Water-Containing Calcium Carbonates and Their Transformations into Amorphous and Crystalline Carbonate Modifications

Kende Attila Béres [1,*], Péter Németh [2,3] and László Kótai [1,*]

[1] Institute of Materials and Environmental Chemistry, HUN-REN Research Centre for Natural Sciences (MTA Centre of Excellence), 1117 Budapest, Hungary
[2] Institute for Geological and Geochemical Research, HUN-REN Research Centre for Astronomy and Earth Sciences (MTA Centre of Excellence), 1112 Budapest, Hungary; nemeth.peter@csfk.org
[3] Research Institute of Biomolecular and Chemical Engineering, Nanolab, University of Pannonia, Egyetem út 10, 8200 Veszprém, Hungary
* Correspondence: beres.kende.attila@ttk.hu (K.A.B.); kotai.laszlo@ttk.hu (L.K.)

Abstract

Calcium carbonate ($CaCO_3$) is a dominant component of sedimentary rocks and biogenic structures, and is one of the most frequently studied inorganic compounds. It also plays a key role in preparing modern engineered materials. $CaCO_3$ has three well-known polymorphs, calcite, aragonite, and vaterite, and four solvatomorphs with diverse crystallographic arrangements, hydration states, reactivity, and stability. Its solvatomorphs include the variable water-containing amorphous calcium carbonate (ACC—$CaCO_3 \cdot xH_2O$) and the crystalline monohydrocalcite (MHC—$CaCO_3 \cdot H_2O$), calcium carbonate hexahydrate (ikaite—$CaCO_3 \cdot 6H_2O$), and the recently reported hemihydrate (CCHH—$CaCO_3 \cdot 0.5H_2O$). Here, we review the preparation, crystal structure, and properties of these solvatomorphs and discuss their mutual transformations.

Keywords: calcium carbonate; solvatomorphs; amorphous calcium carbonate (ACC); ikaite; monohydrocalcite; hemihydrate; mutual transformations; crystal structure

check for updates

Academic Editor: Duncan H. Gregory

Received: 7 August 2025
Revised: 9 September 2025
Accepted: 22 September 2025
Published: 28 September 2025

Citation: Béres, K.A.; Németh, P.; Kótai, L. Review on Chemistry of Water-Containing Calcium Carbonates and Their Transformations into Amorphous and Crystalline Carbonate Modifications. *Inorganics* **2025**, *13*, 321. https://doi.org/10.3390/inorganics13100321

Copyright: © 2025 by the authors. Licensee MDPI, Basel, Switzerland. This article is an open access article distributed under the terms and conditions of the Creative Commons Attribution (CC BY) license (https://creativecommons.org/licenses/by/4.0/).

1. Introduction

Calcium carbonate ($CaCO_3$) is one of the most important inorganic compounds, playing a key role in geology [1], biology [2,3], and industry [4–7]. It is prevalent in sedimentary rocks [8–10], biogenic structures [11–13], and even in modern engineered materials [14,15]. In spite of its simple composition, $CaCO_3$ has a variety of polymorphs and solvatomorphs. Polymorphs are anhydrous forms, whereas solvatomorphs are hydrated calcium carbonates, and these terms are used interchangeably in the text. The diversity in crystallographic arrangements and hydration states results in unique occurrences and distinct properties, including reactivity and stability [16]. In addition to the well-known calcite, aragonite, and less-known vaterite polymorphs, the hydrated forms, including the variable crystalline water-containing amorphous calcium carbonate (ACC—$CaCO_3 \cdot xH_2O$) [17] and the crystalline monohydrocalcite (MHC (also called hydrocalcite)—$CaCO_3 \cdot H_2O$) [18], calcium carbonate hexahydrate (ikaite)—$CaCO_3 \cdot 6H_2O$ [19], and the recently reported hemihydrate (CCHH—$CaCO_3 \cdot 0.5H_2O$) [20], are the focus of intense investigations [2,21–25]. Each solvatomorph is characterized by a unique structure and hydrogen-bonding systems [24,26–30]. They differ not only in their crystalline water content, but in their long-range ordering [31–33], solubility [34–39], and transformation pathways [11,21,40–46].

Fundamental principles such as formation energy and stability of water-containing ACC are crucial for understanding its stability and mutual interconversion pathways among ACC, crystalline solvatomorphs, and anhydrous polymorphs [21]. Here, we review the occurrence, preparation, crystallography, spectroscopy, computational analysis, and thermodynamics of various carbonate forms [38,41–50]. We summarize and compare the properties of amorphous and crystalline calcium carbonate solvatomorphs and provide insights into their transformation routes.

2. Occurrence in Geological Environment and/or Biological Systems, and Preparation, Morphology, and Properties of Hydrated Calcium Carbonates

Calcite, aragonite, and vaterite are anhydrous compounds; however, studies of their atomic force microscopy (AFM) demonstrated that they may acquire adsorbed water layers when exposed to ambient and wet atmospheric conditions or aqueous environments [51–53]. At ambient conditions, the stable form is calcite, and the metastable vaterite and aragonite transform to calcite on contact with water [54].

2.1. Ikaite

The preparation of ikaite preceded its natural discovery. Ikaite was synthesized in 1865 by Pelouze in the reaction of a carbonic acid stream and lime water ($Ca(OH)_2$ solution) at around 0 °C [55], and the "ikaite" name was given when it was identified in the Ikka fjord (Grönland) by Pauly in 1963 [56]. Its water content was first determined as five moles [57]; however, Johnston et al. (1917) demonstrated that the material, prepared from a mixture of 0.1 M of $CaCl_2$ and K_2CO_3, buffered with KOH solution (2 g in 600 cm^3) at 2 °C, contains six moles [58]. Interestingly, needle-like "ikaite" crystals were found by Iwanoff in a Paleocene marl even in 1906, close to Puławy, Poland [59]; however, its composition was believed to be $CaCO_3 \cdot 5H_2O$. After the discovery of natural ikaite in the Ikka fjord, many other cold-place occurrences were identified, like the Antarctic ice (Suess et al. [9]), Mono Lake (California, USA) (Bischoff et al. [60]), the Scarisoara Ice Cave (Romania) (Onac et al. [61]), alkaline artificial riverbeds (Austria) (Boch et al. [62]), and sea sediments (Rogov et al. [50]). Other occurrences include biogenic materials (Larsen [47], Mikkelsen et al. [63], Swainson et al. [64], Rickaby et al. [65], Garvie et al. [66]), washed-rind cheese [67], and steel waste leachate (Bastianini et al. [68]). Ikaite is stable <4 °C, and above this temperature it starts to decompose into calcite. However, its decomposition was confirmed even at −20 °C by solid-state NMR studies [17]. Ikaite has been used as an indicator of cold paleotemperatures (Larsen [47], Swainson and Hammond [64], and Rickaby et al. [65]). Calcite pseudomorphs after ikaite are commonly called glendonites, which have been from marine clastic rocks, caves, and lacustrine sediments (Larsen [47], Tollefsen et al. [69], Németh et al. [70], Schultz et al. [71]), and their occurrence has been correlated with cold environments and has attracted the attention of paleoclimate researchers (De Lurio and Frakes [48], Rogov et al. [50]).

Ikaite can be prepared in many ways [21,58]. For example, following the method of Johnston et al. [58], Bischoff et al. mixed dropwise a 0.1 M solution of $CaCl_2$ and K_2CO_3 with a 0.04 M KOH solution at 0 °C and prepared 10 g of ikaite under 6–8 h [60]. Lázár et al. also followed the procedure described by Johnston et al. [58], and successfully prepared ikaite at pH 12.7 and at temperatures between 0 and 4 °C. They demonstrated that ikaite could also be synthesized by mixing 0.02 M Na_2CO_3 and 0.02 M $CaCl_2$ solutions, ageing the mixture at 0–4 °C for 20–25 min, and quickly vacuum filtering the precipitated material [21]. An alternative method for ikaite synthesis is based on alkalizing a cold (2 °C), nearly pH-neutral $Ca(HCO_3)_2$ solution with solid KOH [72]. Following the procedure, ikaite

can be synthesized at pH 12.1, 10.3, and 9.1. Tollefsen et al. showed that ikaite can be prepared at 35 °C between pH 9.3 and 10.3 by mixing natural seawater and a Na_2CO_3-rich solution [69]. Hu et al. synthesized ikaite at temperatures between 0 and 4 °C and at pH between 8 and 10 by mixing 2.5 M $CaCl_2 \cdot 2H_2O$, 0.5 M $NaHCO_3$, and 0.5 M NaOH solutions and seawater—a similar mixture, prepared from distilled water containing NaCl, $MgCl_2$, Na_2SO_4, KCl, $SrCl_2$, KBr, and H_3BO_3 in various ratios [73].

Ikaite crystals are commonly prismatic and characterized by pyramidal morphology (Figure 1A). In fact, the steep and spiky canted tetragonal pyramids are uniquely preserved in glendonites (Németh et al. [70], Schultz et al. [71]) and can be associated with the precursor ikaite. In addition to prismatic grains, ikaite could also occur as platy crystals. Lázár et al. [72] demonstrated that alkalizingto a nearly pH-neutral $Ca(HCO_3)_2$ solution with solid KOH results in flakes with lateral dimensions of 5–10 μm and thicknesses of 0.1–0.5 μm.

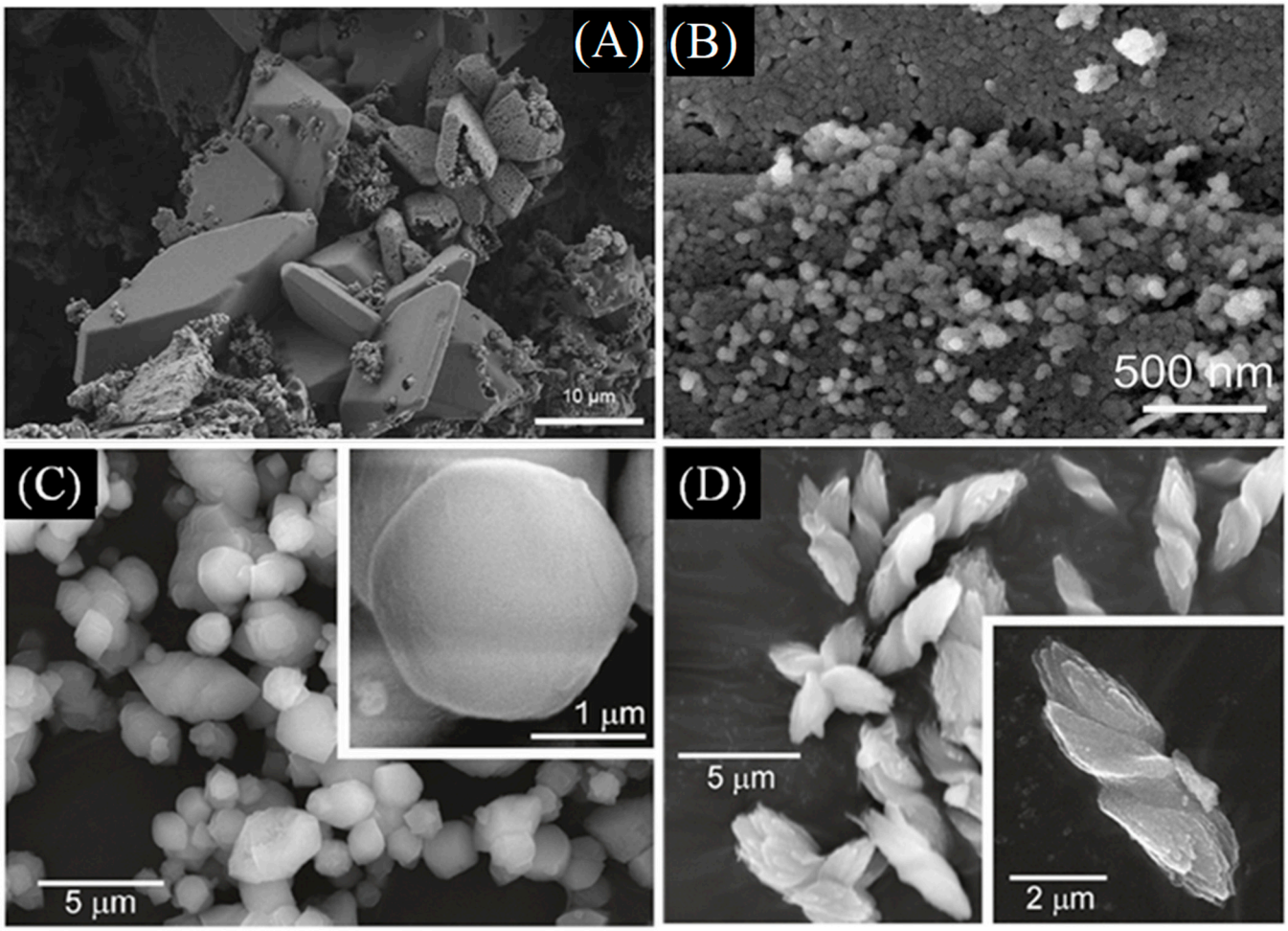


Figure 1. The typical morphology of different hydrated $CaCO_3$ (SEM images). Ikaite crystals with cavities (**A**), reproduced from Tollefsen et al. with permission [69]. ACC crystals (**B**), reproduced from Lázár et al. [72] with permission. The distinct morphology of MHC grains, prepared in 20 mol% Mg-containing mother liquor at 288 K (**C**) and 303 K (**D**), reproduced from the work of Kimura et al. [74] with permission.

2.2. Monohydrocalcite, MHC

Monohydrocalcite or hydrocalcite, identified as $CaCO_3 \cdot H_2O$, was first synthesized in the reaction of Na_2CO_3 and $CaCl_2$ by Brooks et al. (used 2 to 1 molar ratios) [75] and Van Tassel et al. (used 4 to 1 molar ratios) [76] in 1950 and 1962, respectively. The synthesis required $MgCl_2$ presence > 200 ppm. MHC was first found in nature by Sapozhnikov

et al. in Lake Issyk-Kul (Kyrgyzstan) [77] and later by Carlström in fish otoliths [78] in 1959 and 1963, respectively. MHC was also reported in a submarine ikaite tufa column around the Arctic Ikka Fjord, Greenland [79]. The formation of MHC was found in the air scrubbers of different air-conditioning plants [80] Garvie reported its occurrence from the decay of the saguaro cactus [81], Zaytseva et al. found in the microbialites from Laguna de Cisnes [82], and Krauss et al. noted that certain evaporitic settings and lacustrine environments produced a calcium carbonate deposit, of which diffraction patterns were not similar to calcite or aragonite [18], but agreed well with that of MHC, prepared by mixing sea water and K_2CO_3 [83].

Duedall et al. [84] detected a delayed precipitation of MHC after 8 h at 20 °C, and, as Nathana mentioned earlier [85], the diffraction patterns of this product do not agree with those of the expected vaterite [84]; therefore, Duedall et al. concluded that it was a new kind of material, MHC [84]. Vereshchagin et al. found that transition metal-containing solutions can facilitate the formation of MHC [86]. Rodriguez-Blanco et al. prepared MHC at 21 °C by mixing 1 M Na_2CO_3 solution with 700 mM $CaCl_2$ and 300 mM $MgCl_2$ solutions. They found that the $MgCl_2$ solution promotes the formation of MHC [87]. Kitajima et al. followed the same method, but performed the synthesis at 5 °C [88]. Zhang et al. prepared MHC in the following way: they mixed $Na_2Si_3O_7$ (sodium silicate) solution (varying between 1 and 10 v/v%) with 0.05 M Na_2CO_3 solution and added 1M HCl solution to the mixture, that resulted in a gel. Into this gel, a 0.05 M $CaCl_2$ solution was injected (at pH = 10.5), and, due to the diffusion of the Ca^{2+} ion in the silicone gel, it resulted in MHC crystals after a day [89]. Kralj et al. prepared MHC under a night by mixing 0.3 g K_2CO_3 with a 250 mL seawater-similar mixture, prepared from triple-distilled water containing 29.2 g NaCl, 5.0 g $MgCl_2$, 1.1 g $CaCl_2$, and 0.024 g $SrCl_2$ in 1000 mL triple-distilled water [90].

Taylor reported that MHC crystals, precipitated from saline lake water, are hard pelletal aggregates with a sponge-like texture [91]. Dahl and Buchardt [79] demonstrated that MHC from the Arctic Ikka Fjord is associated with ikaite and occurs in three different forms as (1) spherulites, (2) subhedral to euhedral crystals, and (3) zoned euhedral crystals. According to Kimura et al. [74], synthetic MHC either consists of well crystalline spherical particles (Figure 1C) or poorly crystalline aggregates of twisted spindles (Figure 1D).

2.3. Calcium Carbonate Hemihydrate, CCHH

The discovery of calcium carbonate hemihydrate (CCHH, $CaCO_3{\cdot}0.5H_2O$) [20] represents a critical missing link in the hydration–dehydration transitions of calcium carbonate containing hydrated phases. First, it was synthesized by Zou et al. in magnesium-rich aqueous systems [20], and recently, it was reported in fresh coral skeleton and nacre surfaces [22]. The high-resolution X-ray powder diffraction (HRXRPD) and automated electron diffraction tomography (ADT) measurements revealed that CCHH has a monoclinic lattice (space group found to be space group $P2_1/c$) and the 0.5 molar crystalline water was proved by TGA studies [20].

The stability and the electronic and mechanical properties of CCHH were determined by DFT (PBE + TS) calculations [92]. The Gibbs energy was found to be −0.052 eV/atom, for the following proposed equation:

$$CaCO_3 + 0.5\ H_2O = CaCO_3{\cdot}0.5H_2O \quad (1)$$

which is higher than the −0.055 and −0.139 eV/atom values, calculated for the MHC and ikaite, respectively [92]. The compressibility of the CCHH is large due to the monoclinic structure and is found to be 109.28 and 129. 65 GPa under the external uniaxial stress along the [001] and [010] directions, respectively, whereas, in the case of the ikaite and MHC, these values were only 48.32 and 88.97 for [001] and 91.21 and 80.81 GPa for [010],

respectively [92]. The Young's modulus was calculated to be 60.51 GPa (these values were 36.56 and 91.28 GPa for MHC and ikaite, respectively) [92].

The synthesis of CCHH is based on mixing a 5–100 mM $Na_2CO_3 \cdot 10H_2O$ solution with a solution containing $MgCl_2 \cdot 6H_2O$ and $CaCl_2 \cdot 2H_2O$ (Mg^{2+} to Ca^{2+} ratio was 5 to 1, ultra-pure water) at room temperature. The precursor ACC transforms to needle-like CCHH crystals after 2000 s if the solution is stored in an air-proof container [20].

2.4. Amorphous Calcium Carbonate (ACC)

One of the most important hydrous $CaCO_3$ is ACC. It lacks long-range ordering and is characterized by variable water content. In nature, ACC was first recognized during the deposition of the crystalline core material of Sponge-Spicules by Minchin in 1909 [93]. In 1912, Kendall emphasized its high instability as he could not determine its water content, but measured the composition of calcite [94]. Dorfmüller found that increasing alkalinity stabilizes the amorphous state [95]. Schmidt [96], Prenant [97], Rinne [98], and Odum [99] found an amorphous phase, which was evidenced by a diffuse scattering pattern of spicules in marine animals. Furthermore, Towe et al. found a similar material by studying the evaporation of seawater [100]. ACC was reported from cave bacteria [101], slime moulds [102], *Pyura pachydermatina tunicates* [103], and *Biomphalaria glabrata* snail embryos [104]. Scientists recognized that many organisms utilize ACC as a transient precursor, which later transforms into a crystalline phase [105–112]). The finding and study of ACC provided new insights into biomineralization [113], sediment formation [114], and atmospheric processes [115–119]. The transformation of the $CaCO_3$ polymorphs plays an important role in biomineralization, and ACC became one of the most commonly used paleoindicators, e.g., of ultra-low-temperature [8,120–123]. Studying carbonate transformation provides key insights into pressing contemporary issues such as climate change and CO_2 utilization, including carbon capture [124–126] and storage (CCS) technologies [127–129].

ACC is a precursor material which rapidly transforms to carbonate polymorphs and solvatomorphs depending on the synthesis conditions. However, its transition can be delayed, and ACC can be stabilized. Successful methods are summarized by Liu et al. [130]. Konrad et al. prepared ACC by mixing equimolar 0.25–0.25 M $CaCl_2$ and Na_2CO_3 solutions at pH > 10, and then rapid filtering and freeze-drying [131]. Lázár et al. [72] reported that 100 nm-sized ACC particles could be prepared by mixing K_2CO_3 and $CaCl_2$ solutions, and rapidly filtering and washing them with cold (2 °C) acetone (Figure 1D). Furthermore, ACC nanoparticles can be prepared in an aerosol-based way by spraying 10–100 µm-sized droplets into CO_2-enriched air from an aqueous 23 mM $Ca(OH)_2$ solution [132,133]. Chen et al. [134] reported an additional gas diffusion method, in which ammonia and CO_2 vapours, generated from ammonium carbonate, diffuse into abs. EtOH and a 0.0136 mM $CaCl_2 \cdot 2H_2O$ solution, leading to the formation of ACC. However, this method was found to be poorly reproducible and resulted in a limited amount of material [134]. Additives such as Mg^{2+} could stabilize ACC [41], and we will review the stabilization process in Section 4. Selected synthetic routes are summarized in Table 1.

ACC commonly occurs as nm-sized spheres (Figure 1B). However, Lázár et al. [72] demonstrated that rapid dehydration of ikaite by organic solvents and vacuum pumping at room temperature, and by increasing the temperature from 5 to 30 °C within 1 min, results in micron-sized, porous ACC grains that preserve the prismatic ikaite grain morphology.

Table 1. Possible synthetic routes of hydrated $CaCO_3$ solvatomorphs (ikaite, monohydrocalcite, $CaCO_3$ hemihydrate, and amorphous $CaCO_3$). We highlighted the presence of other ions (like Mg^{2+}) due to their importance.

Name	Method 1	Method 2	Method 3
Ikaite	0.1 M $CaCl_2$ + 0.1 M K_2CO_3 + 0.04 M KOH; T = 0 °C [60]	0.02 M Na_2CO_3 + 0.02 M $CaCl_2$; pH = 12.8; T = 0–4 °C; t = 20–25 min [21]	2.5 M $CaCl_2{\cdot}2H_2O$ + 0.5 M $NaHCO_3$ + 0.5 M NaOH + seawater-similar mixture (presence of, e.g., **PO_4^{3-}**), T = 0 and 4 °C [73]
Monohydrocalcite (MHC)	700 mM Na_2CO_3 + 700 mM $CaCl_2$ + **$MgCl_2$ (or $CoCl_2$ $2H_2O$** [86]); T = 5 or 21 °C [87,88]	0.05 M Na_2CO_3 + sodium silicate gel with 0.05 M $CaCl_2$; pH = 10.5 [89]	0.3 g K_2CO_3 + 250 mL seawater-similar mixture [90]
Calcium carbonate hemihydrate (CCHH)	5–100 mM Na_2CO_3 ·$10H_2O$ + **$MgCl_2{\cdot}6H_2O$** + $CaCl_2{\cdot}2H_2O$ (**Mg^{2+} to Ca^{2+} ratio was 5 to 1**); T = 25 °C; t = 4200 s [20]	------	------
Amorphous Calcium carbonate (ACC)	0.25 M $CaCl_2{\cdot}2H_2O$ + Na_2CO_3, pH~10; T = 20 °C, filtration and freeze-drying [131]	23 mM $Ca(OH)_2$ solution, microfluidic spray-drying [132,133]	Gas diffusion of NH_3/CO_2 through 0.0136 mM $CaCl_2{\cdot}2H_2O$ in abs. EtOH, pH~8 [134]

3. Spectroscopic and Structural Studies on Hydrated Calcium Carbonates

3.1. IR and Raman Spectroscopy

Raman and IR spectroscopies are excellent techniques to study the different polymorphs and solvatomorphs of $CaCO_3$ (Figure 2). These techniques can detect the vibrational modes of carbonate and water (Table 2), confirming that while local arrangements resemble those of crystalline calcium carbonate, the overall structure is disordered [135]. For example, ikaite and MHC can easily be distinguished by IR and Raman spectroscopy. The υ_s (O-H) stretching modes of ikaite appear as multiple bands between 3550 and 3200 both in IR and Raman spectra [136], whereas MHC gives rise to three well-separated υ_{OH} modes at 3400, 3327, and 3236 cm^{-1} in the IR spectrum (Table 2) [136]. Coleyshaw et al. found well-resolved Raman bands for ikaite and MHC at 3423, 3240, and 3182 cm^{-1} and 3425, 3326, and 3224 cm^{-1}, respectively [136]. CO_3^{2-} modes are positioned between 1500–1400 cm^{-1} ($\upsilon_{as,CO}$) and 1100–1050 cm^{-1} ($\upsilon_{s,CO}$), at ~870 cm^{-1} ($\pi_{,CO}$), 760, and 725–690 cm^{-1} ($\delta_{as,CO}$) [136] for both compounds. The IR and Raman data of hydrated $CaCO_3$ compounds are listed in Table 2 [136].

Table 2. The bands in the IR and Raman spectra of the different hydrated $CaCO_3$ solvatomorphs (ikaite, monohydrocalcite, $CaCO_3$ hemihydrate, and amorphous $CaCO_3$). Reproduced from Coleyshaw et al. [136] and Zou et al. [20].

Modes	Ikaite [136]		MHC [136]		ACC (Hydrated)		CCHH [20]	
	IR	Raman	IR	Raman	IR [138]	Raman [139]	IR	Raman
$\upsilon_{as,OH}$	3543, 3502, 3468, 3404, 3361, 3119	3423, 3182	3400, 3327	3425, 3326	3401, 3130	3430	3379	3382
$\upsilon_{s,OH}$	3216	3240	3236	3224	3226	---	3290	3285
$\delta_{s,HOH}$	1673, 1644, 1616	---	1700	---		1650	1659	1661
$\upsilon_{as,CO}$ (υ_3)	1425, 1411	1483	1492, 1401	---	1485	1540, 1460, 1390	1524, 1490, 1423, 1392,	1579, 1483, 1423

Table 2. *Cont.*

Modes	Ikaite [136]		MHC [136]		ACC (Hydrated)		CCHH [20]	
	IR	Raman	IR	Raman	IR [138]	Raman [139]	IR	Raman
$\upsilon_{s,CO}$ (υ_1)	1085	1072	1063	1069	1064	1077	1096	1102
$\pi_{,CO}$ (υ_2)	876	873	872	876	876, 856	868	866, 860	862
$\delta_{as,CO}$ (υ_4)	743, 720	722	762, 698	723, 699	698	723, 698	723, 692	731, 700

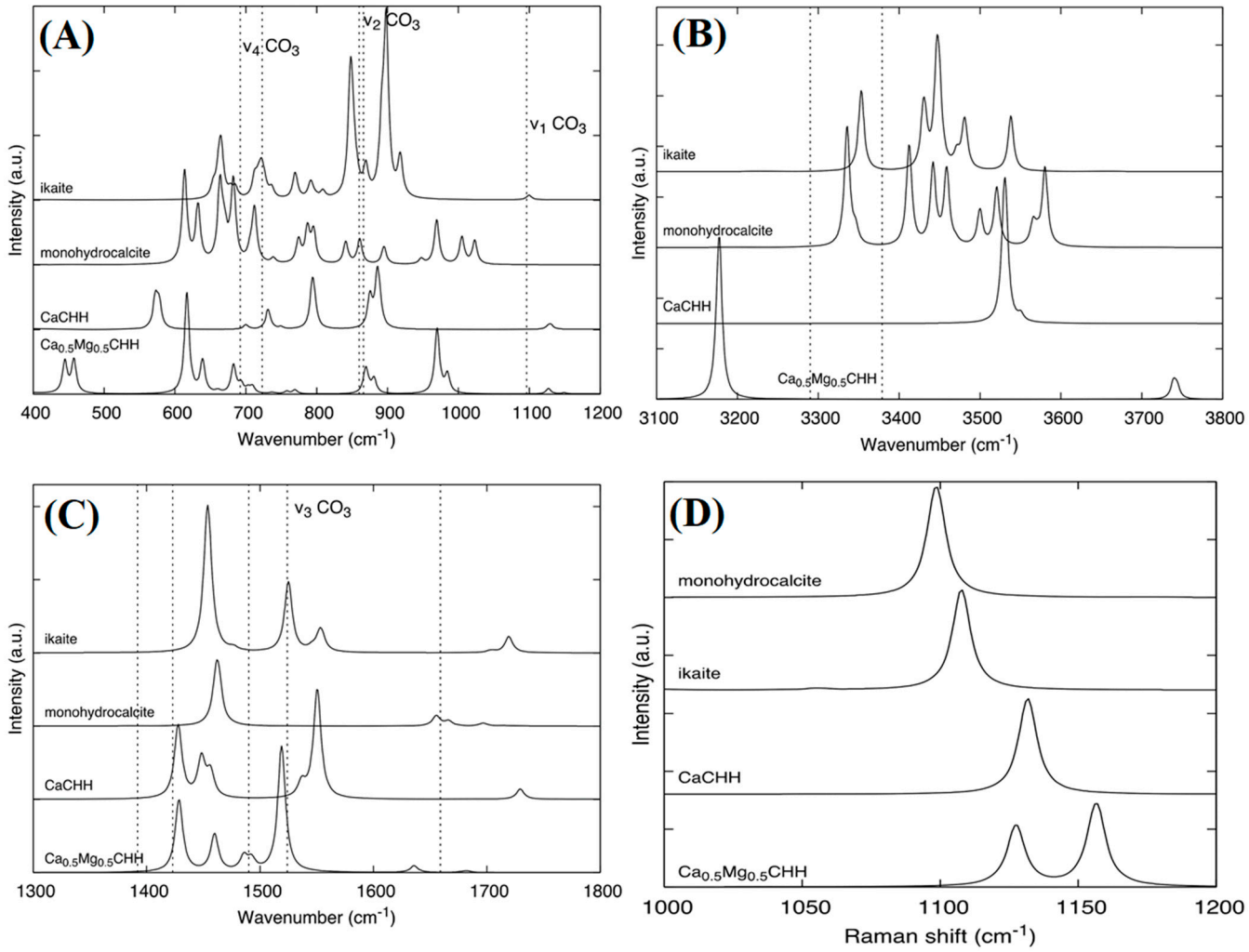


Figure 2. The characteristic bands of the different hydrated $CaCO_3$ in the IR (**A**–**C**) and Raman (**D**) spectra and the effect of the addition of Mg^{2+} on the peak position of the CCHH (note that here it is marked as CaCHH). Reproduced from Aufort et al. work [137] with permission.

Effenberger and Coleyshaw et al. showed that the IR and Raman studies can be used to identify and distinguish MHC from ikaite and CCHH (Table 2) [136,140,141]. Solid-state NMR studies of MHC confirmed the presence of H_2O and CO_3^{2-} ions in different chemical environments [17].

3.2. Structure of Ikaite

Ikaite has monoclinic ($C2/c$) flat, platy, or tabular crystals with a prismatic habit, both at −120 °C (Dickens et al. [142]) and −25 °C (Hesse et al. [143]). Its main crystallographic parameters are summarized in Table 3 in comparison to MHC and CCHH.

Table 3. Crystalline parameters of the different hydrated $CaCO_3$ solvatomorphs (ikaite, monohydrocalcite, and $CaCO_3$ hemihydrate).

Name	Calcium Carbonate Hexahydrate [143]	Monohydrocalcite [140]	Calcium Carbonate Hemihydrate [20]
Acronym	Ikaite	MHC	CCHH
Formula	$CaCO_3 \cdot 6H_2O$	$CaCO_3 \cdot H_2O$	$CaCO_3 \cdot 0.5H_2O$
Shape of the crystalline	flat, platy, or tabular crystals with a prismatic habit	thin, sometimes rounded or plate-like crystals	needle-like morphology
Crystal System	Monoclinic	Trigonal	Monoclinic
Space group	$C2/c$	$P3_1$	$P2_1/c$
Lattice parameters	a = 8.78 Å b = 8.28 Å c = 10.88 Å β = 109.59°	a = 10.554 Å b = 10.554 Å c = 7.454 Å	a = 9.33 Å b = 10.44 Å c = 6.16 Å β = 90.5°
Unit Cell Volume (Å^3)	~743.7	~751.6	~600.0

The structure of ikaite is composed of hydrated calcium carbonate chains, aligned along the axis *a* and linked together by a hydrogen bond system [144]. The thermal expansion of the unit cell and its relationship with the hydrogen-bonding system of ikaite were studied by several groups. Swainson et al. used neutron powder diffraction between 4 and 270 K [64], Lennie et al. applied synchrotron X-ray powder diffraction (S-PXRD) [144] between 114 and 293 K, and Tateno et al. performed Single-Crystal X-ray Diffraction (SC-XRD) [145] studies between 223 and 263 K. Temperature increase results in anisotropic unit cell expansion of ikaite along the *a* and *c* axes (Table 3). The largest structural modification occurred near the dehydration temperature of the ikaite, which suggests that the water, and especially the H-bonding system, is a strong cohesive force in the structure [145]. Chahi et al. refined the structure parameters of ikaite by DFT calculations. They have found that the *a*, *b*, and *c* cell parameters increased by +1.7, +0.4, and +0.03% applying DFT-PBE calculation and decreased by −1.1, −0.5, and −1.4% applying DFT-D2 calculation as a result of the differences in the van der Waals interactions [146]. Rietveld structural refinement of PXRD data, applying the structure model determined by Hesse [143], resulted in Ca-$O_{carbonate}$ distances of 2.43–2.44 Å [66,75]. The strong anisotropic thermal expansion suggested the H-bonds play an important role in the structure; therefore, neutron diffraction measurements were performed to determine the positions of the H(D) atoms in the structure. The D-O distances varied between 1.761 and 1.962 Å in the ikaite structure (Figure 3A), and the hydrogen bond distance between the D3 and O2 atoms was found to be 2.508(9) Å [64,144].

Further neutron diffraction studies on ikaite showed the precise locations of hydrogen atoms within the lattice, clarifying the unique arrangement of water molecules [17,147]. The presence of six water molecules results in a looser, more open structure compared to anhydrous carbonates, and they are responsible for the high reactivity and sensitivity to temperature and anisotropic thermal expansion. The structure of ikaite was refined with DFT calculations as well, in a detailed manner [146,148]. Costa et al. performed DFT-GGA-PBE calculations and found that the band gap of ikaite did not change compared to calcite, but the band type changed to direct from indirect (Figure 4) [148]. The complex electronic structure of calcite was simplified upon hydration, and only two flat bands were formed very close to each other in the case of MHC and a single band in the case of ikaite (Figure 4B,C) due to the O_{2p} states of crystalline water. The simplification of the electronic structure results from a structural rearrangement due to the entrance of crystalline water [148]. Furthermore, this simplification implies that water molecules more strongly and directly influence the electronic structure of ikaite compared to MHC [148].

The calculated elastic data are in good agreement with the experimental elastic parameters obtained by Sekkal et al. [28]. In the case of ikaite, a smaller (5.069 eV instead of 5.14 eV) value was obtained by Zhou et al. by DFT-PBE + TS calculations [92].

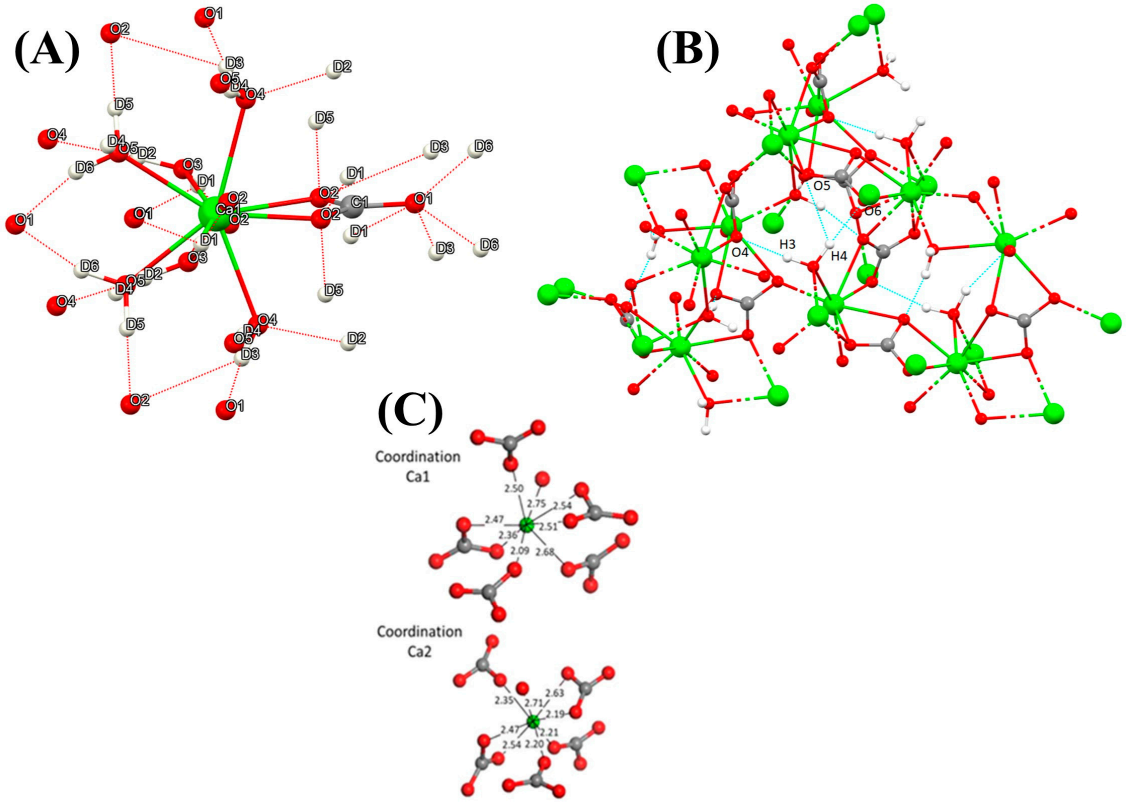


Figure 3. The structure and H-bond system of ikaite, reproduced from Lennie et al. Rietveld structural refinement work [144] and from ICSD 98370 (**A**). The structure and H-bonding system of MHC, reproduced from Rietveld structural refinement from ICSD 160811 (**B**). The crystalline structure of CCHH, which shows the coordination spheres and Ca-$O_{carbonate}$ distances, reproduced from Zou et al. [20] with permission (**C**). The colour code of the atoms is the following: ● carbon, ● hydrogen, ● oxygen, and ● calcium.

3.3. Structure of MHC

MHC adopts a trigonal lattice (space group $P3_1$) similar to calcite (Table 3) [140,149,150]. Its structure is similar to that of ikaite, as the Ca^{2+} ion is surrounded by eight oxygen atoms, i.e., can be considered as a distorted tetragonal antiprism, and shares two O-O edges between the Ca coordination polyhedron and a carbonate group (Figure 3B). A primitive trigonal supercell was also detected but could not be determined properly; the proposed space group was $P3_1$ with a = 10.5536 Å and c = 7.5446 Å. The Ca-$O_{carbonate}$ distances are between 2.41 Å and 2.47 Å, and the two Ca-O(w) distances are 2.49 Å (Figure 3B) [149].

Swainson et al. performed X-ray and neutron powder diffraction studies and Rietveld structure refinement on natural MHC samples from South Australia [149]. The $P3_1$ structure model consisted of three independent networks [149]. There was one water molecule and one carbonate group (Figure 3B) in each network, and every hydrogen atom of water molecules belonged to two different hydrogen bond systems, including a linear one (H3···O4) with one carbonate ion and a second one showing a bifurcated hydrogen (H3···O5 and H3···O6) bond to another carbonate ion (Figure 3B) [149]. The same interaction was detected by Makovicky, who described the structure of MHC as consisting of rods with three different Ca^{2+} ions, accompanied by spiral arrangements of CO_3^{2-} ions and crystalline water molecules [151]. These alternating carbonate environments in

MHC were also detected by ESR (electron spin resonance) and 1H ENDOR (electron-nuclear double resonance) (accompanied by TGA) studies performed by Callens et al. [151]. The water molecule in the structure of MHC is coordinated in a manner that facilitates extensive hydrogen-bonding interactions with surrounding carbonate oxygens, thereby modifying the local geometry and overall lattice dynamics. The lattice and structural relations were studied by Demichelis et al. with the DFT computation method at the PBE0 level of theory, using all-electron Gaussian-type basis sets [152,153]. The calculated structural parameters were in good agreement with the experimental ones (Table 3 [149]), e.g., the 8-fold Ca coordination sphere and the shortest distance between two water molecules was at least 4 Å; each water molecule has two H-bonds with two different carbonate ions [152,153]. The calculation, similar to the measurement, also showed that there was a three-fold rotational axis parallel to the *c* lattice parameter, which created a triangular motif projected on the plane perpendicular to the [001] direction [149]. However, the calculation indicated that the symmetry of the "helical" chains, similar to what occurs in vaterite, could rather be described with the space group of $P3_1$ or $P3_2$ [153]. The occurrence of these helical chains might explain why ACC transforms into calcite or aragonite via MHC and vaterite intermediate phases [153]. The nature of van der Waals interactions was also studied by DFT-GGA-PBE calculation, and found that the presence of water increased the main band gap of MHC by 0.4 eV relative to the anhydrous structure (Figure 4) [148]. The structural parameters of the MHC were refined by DFT-PBE (standard) and -D2 (dispersion-corrected) methods [146]. Calculation demonstrated that the *a*, *b*, and *c* cell parameters increased by +0.7, +0.7, and +0.9% applying the DFT-PBE method and decreased by −0.4, −0.4, and −0.09% applying DFT-D2 calculation as a result of the differences in the van der Waals interactions [146]. The values of elastic moduli of MHC were reported to be lower than those of calcite, which is explained by the difference in the strength of the ionic (calcite) and hydrogen (hydrated phase) bonds [146]. Furthermore, MHC has greater elastic moduli, acoustic wave velocities, and Debye temperature than ikaite due to the distinct complex hydrogen-bonding network [146].

The electronic properties of MHC were determined by GGA-PBE (Costa et al., Figure 4B) [148] and PBE + TS calculations (Zhou et al.) [92], and the slightly different band gaps of 5.53 and 5.366 eV, respectively, were explained by the different O_{2p} states [92,148].

3.4. Structure of CCHH

The CCHH has needle-like monoclinic ($P2_1/c$) crystals (Table 3), and in its structure, each Ca^{2+} ion is surrounded by eight oxygen atoms, and the Ca-$O_{carbonate}$ distances were similar to those of other solvatomorphs and varied between 2.09 and 2.68 Å (Figure 3C) [20]. This structural arrangement contributes to the unique hydration state of CCHH, positioning it as an intermediate phase among the amorphous or fully hydrated states (such as ACC and ikaite) and the anhydrous crystalline polymorphs (like calcite). Under ambient conditions, CCHH is metastable; however, the presence of Mg^{2+} ions can stabilize it. The orientation of the water molecules in the structure remained unresolved [20], which prompted Aufort et al. to study the structure of CCHH with Force Field-Based (FF) and PBE0-DC (DFT) geometry optimization methods. Aufort et al. determined CCHH has an orthorhombic *Pbcn* space group instead of the monoclinic $P2_1/c$ [137], and the crystalline water forms hydrogen-bonding interactions. This water lies within channels parallel to the *b*-axis (Figure 3C), unlike ikaite, where water molecules form part of the rigid coordination environment, or monohydrocalcite, where water is more loosely associated [137]. Aufort et al. suggested that some Mg substitution resulted in β angle distortion and lowered the symmetry compared to pure CCHH [137]. The electronic properties of CCHH were determined by DFT (PBE + TS) calculation, and found that the band gap of the O_{2p} orbital was around 4.571 eV, which was much smaller than those in ikaite and MHC [92].

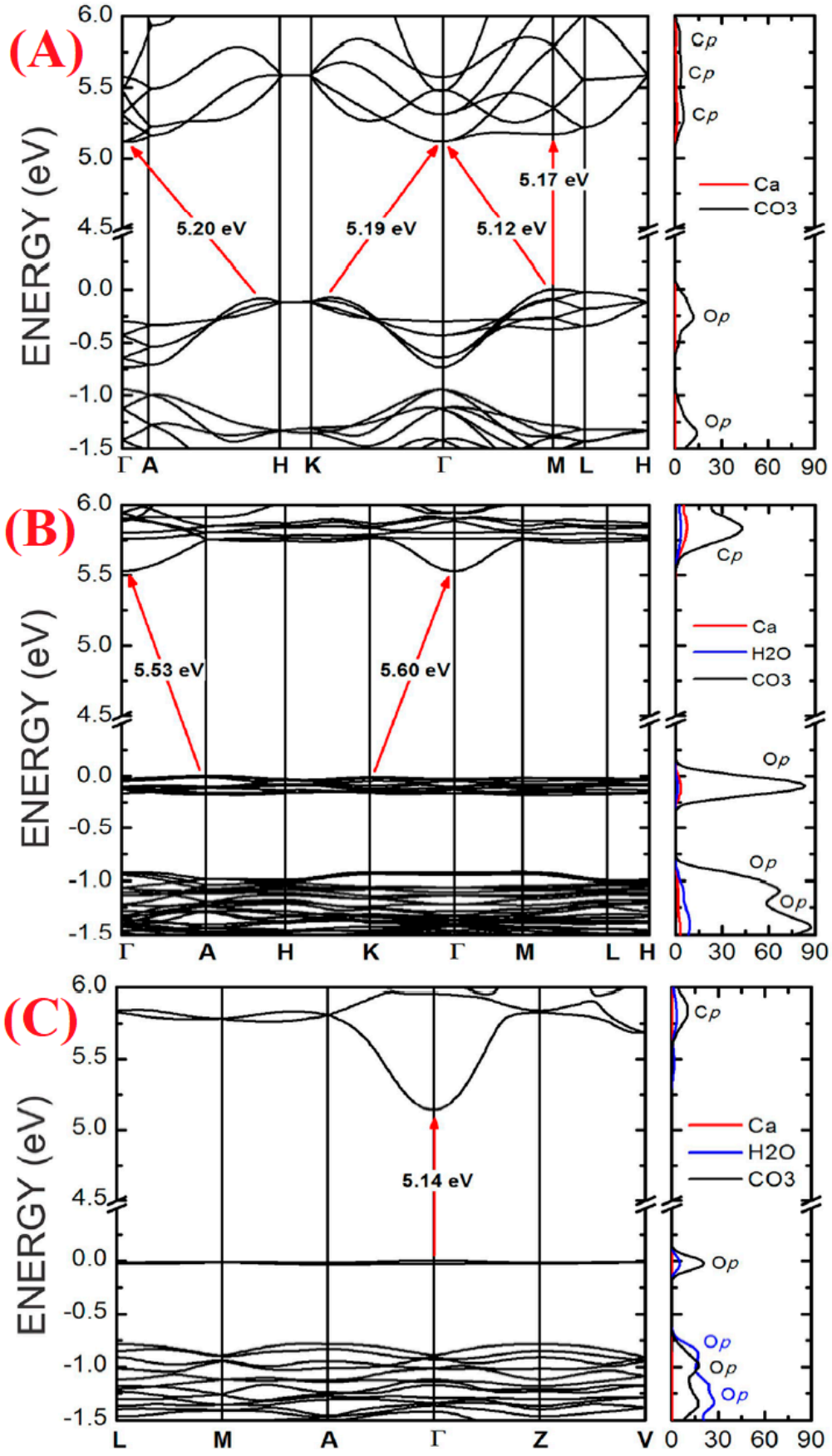


Figure 4. Kohn-Sham band structures (left) and partial densities of states (right) of calcite (**A**), MHC (**B**), and ikaite (**C**). Reproduced from Costa et al.'s work with permission [148].

3.5. Structure of ACC

X-ray, electron, or neutron diffraction studies demonstrated that only a short-range order can be found in the ACC structure [96–99]. In spite of the long-range periodicity, X-ray absorption near-edge structure (XANES) and extended X-ray absorption fine structure spectroscopy (EXAFS) demonstrated that ACC has an MHC and anhydrous $CaCO_3$ similar coordination environments, and water molecules occur in the close proximity to Ca^{2+} and CO_3^{2-} clusters [31–33]. The oxygen K-edge and calcium L-edge EXAFS data showed a close structural relationship among the $CaCO_3$ polymorphs, ACC, and MHC (Figure 5) [33].

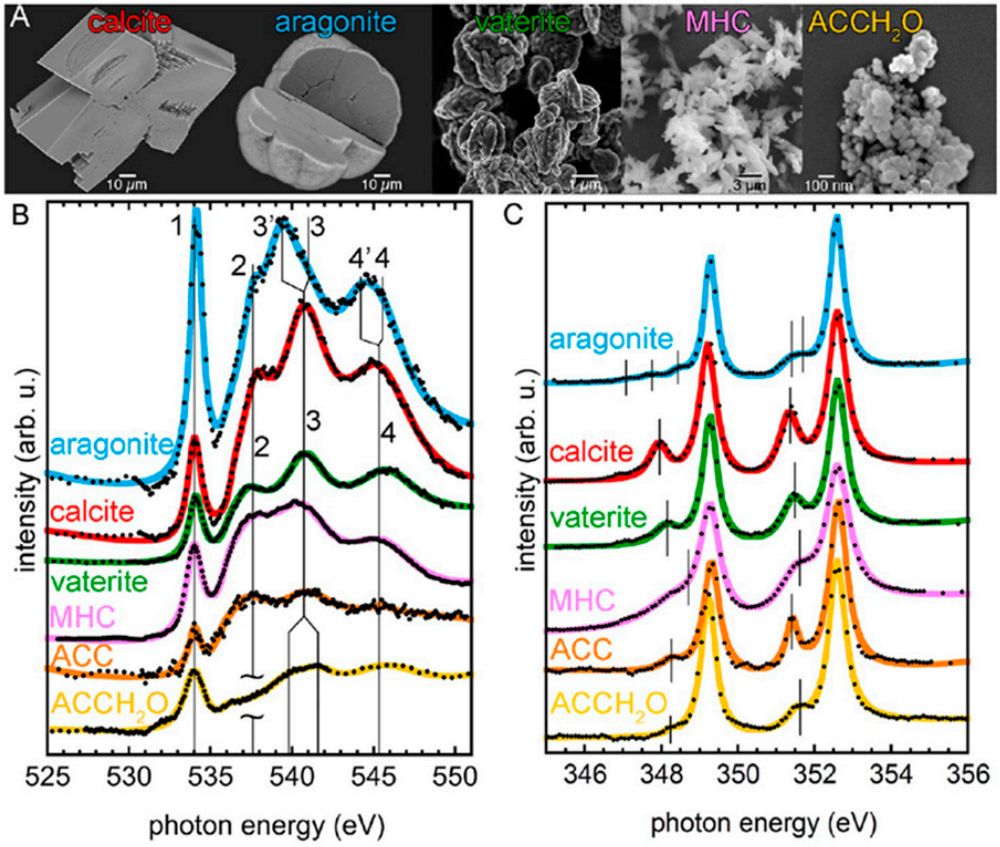


Figure 5. SEM pictures of the calcite, aragonite, vaterite, MHC, anhydrous ACC, and hydrated ACCs (**A**). The oxygen K-edge (**B**) and calcium L-edge experimental spectra (**C**) of their EXAFS measurements are distinct. ACC-Dehyd and ACC-Hyd mean a dehydrated ACC and a hydrated ACC, respectively. Reproduced from DeVol et al. [33] with permission.

The $CaCO_3 \cdot xH_2O$ formula of ACC could be described as $Ca(OH)(HCO_3)$, but the presence of CO_3^{2-} ion instead of HCO_3^- was proved by solid-state ^{13}C NMR studies. Only one peak appeared at the NMR spectra between 166 and 174 ppm (carbonate ion range) [17]. The same conclusion was given by the ^{1}H and the ^{13}C CP MAS studies [17]. The chemical shift in ^{13}C NMR of ACC is dissimilar to any other known $CaCO_3$ polymorphs and solvatomorphs, and proton NMR shows a peak between 5.0 and 5.6 ppm, whereas the proton of HCO_3^- is expected above 13 ppm [154]. Molecular modelling (MM) and molecular dynamics (MD) studies were also used to determine the basic structural features of ACC [29,155–163]. Bushuev et al. used the MD method and found that the Ca-Ca distances are around 5–7 Å [29], which agreed well with previous findings [164]. Jensen et al. determined the two Ca-O and Ca-Ca distances to be 2.4, 4.0, and 6.2 Å, respectively, by neutron and X-ray total scattering techniques combined with MD studies. The Ca-$O_{carbonate}$ peaks showed two coordination spheres centred at 2.37 and 4.11 Å [165], similar to what was found by Goodwin et al. [157]. Michel et al. determined that the short- and

intermediate-range orders were not extended beyond 15 Å, and the NMR studies showed that most of the hydrogen in ACC occurs as structural water, and the amount of rigid O-H groups was about 7 (±3)% [154]. All these values are similar to the other carbonate phases, except ikaite, which lacks the 4.0 Å Ca-Ca distance [143,154].

The variable water content within ACC is one of its hallmark features and is believed to be a critical factor in its role as a precursor in biomineralization processes. The investigation of its transformations demonstrated the strong influence of pH, temperature, pressure, presence of additives, water content, and mechanical conditions [112,166–170].

Bushuev et al. [29] and Jensen et al. studied the hydrogen bond system of ACC by neutron and X-ray total scattering techniques and molecular modelling (empirical potential structural refinement (EPSR)) [165]. The Ca-O_{water} distances showed one coordination sphere at 2.43 Å, which was a little bit longer than that of ikaite and MHC, whereas the Ca-H_w distance gave rise to a single broad coordination sphere at 2.9 Å [165]. The n = 0.5 and 1.1 values for ACC·$x$$H_2O$, 2.7 and 10% of the water molecules were calculated, respectively, and they were not bound directly to the Ca^{2+} ion, but all the water molecules were coordinated to the carbonate oxygens. Accordingly, two types of hydrogen bonds were identified in ACC: one between the $O_{carbonate}$ and water, and another one between the water molecules (Figure 6).

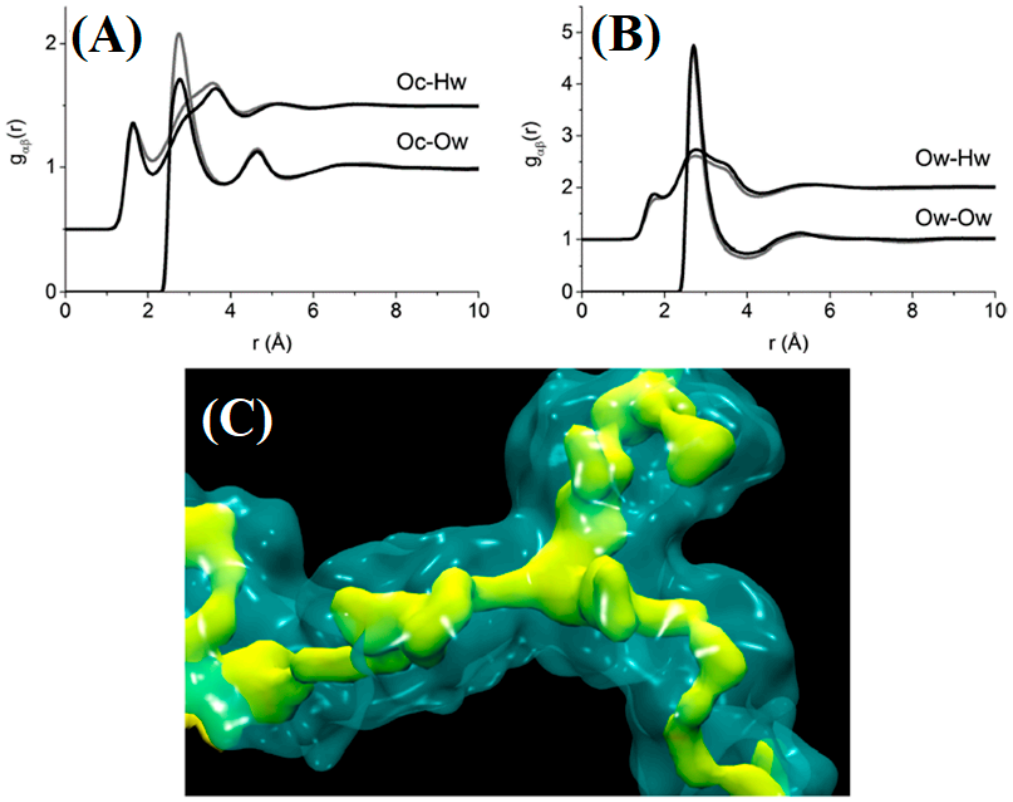


Figure 6. Some of the selected intermolecular partial pair distribution functions (ppdfs) that are related to the hydrogen-bonding systems of the ACC formed between $O_{carbonate}$ and H_{water} (**A**) and between water molecules (**B**). The model of water cluster in the ACC, proposed by Bushuev et al. [29] (**C**). Reproduced from Jensen et al. (**A**,**B**) [165] and Bushuev et al. [29] (**C**) with permissions.

All water molecules have hydrogen bonds with at least one carbonate ion [29,165]. It was concluded that the hydrogen bonds between the $O_{carbonate}$ and H_{water} are more preferable, calculating x = 1 for $CaCO_3$·$x$$H_2O$ [16,142,143], than between water molecules. Additional calculations showed that 63% and 20% of the hydrogen takes part in the carbonate–water and water–water hydrogen bonds, respectively, and these values decreased to 78%

and to 10% upon dehydration, calculating $x = 1$ to $x = 0.5$ for $CaCO_3 \cdot xH_2O$ [165]. These results agreed well with the NMR studies [17,154]. However, there were controversies between Bushuev et al. [29] and Jensen et al. [165] regarding the long-range ordering of the H-bond network in the $CaCO_3 \cdot xH_2O$ systems. Bushuev et al. proposed the presence of water clusters with large numbers in the channels in both ACCs (Figure 6C) [29] (the same was proposed by Gale et al. [156], Goodwin et al. [157], and Innocenti et al. [161]), whereas, Jensen et al. found ca. 220 water molecules (about 80–90% of all water H_2O) in clusters for $x = 1.1$, and not more than 40 water molecules were found in the clusters for $x = 0.5$ in the $CaCO_3 \cdot xH_2O$ system [165].

Katsikopoulos et al. studied the incorporation of foreign ions into calcium carbonate structures, found that Co^{II} ions enter calcite and aragonite, and reported ACC formation at $Co^{II}/Ca^{II} = 5/1$ [171]. Shuseki et al. reported that the Sr^{2+} ions have an influence on the ACC structure [172], and X-ray and neutron diffraction studies aided by MD simulation revealed that the Sr-containing ACC has a partially similar structure to MHC, and, upon the removal of the foreign ion, the structure transformed into calcite [172]. Molnár et al. [173] studied the incorporation of Sr^{2+} and Ba^{2+} in ACC, reported the partition coefficients (D_{Ca}, D_{Sr}, and D_{Ba}) decreased with increasing ionic radius between the solution and the solid, and demonstrated that Sr^{2+} and Ba^{2+} cations significantly modified the structural properties of ACC, and the changes in short-range structure resulted in exceptional kinetic stability of the ternary mixed amorphous Ca–Sr–Ba carbonates.

Lopez-Berganza et al. studied the influence of the amounts (n) of water molecules in the clusters on the stability of $CaCO_3 \cdot xH_2O$ compounds between $n = 1$ and 18 with a combination of Monte Carlo simulation and DFT calculation (DFTB+ and B3LYP) [160]. They found that incremental binding energy (ΔE) became less negative and reached a plateau when n > 11; therefore, water up to n = 12 could fit into the first hydration shell. The simulation proved that for n = 18, 12 water molecules were coordinated to the $CaCO_3$ molecules, and the rest were found in the second hydration shell [160]. Furthermore, incremental binding free energy (ΔG) was close to zero (and even larger) when $n \geq 15$, thus larger clusters were thermodynamically unfavourable in size [160]. The Ca-O_c distance increased with increasing n, and for n > 9, it varied between 2.305 and 2.585 Å, which was in good agreement with the Ca-O_c distances mentioned previously [160].

4. Transformations of Hydrated Calcium Carbonates

The stability of each calcium carbonate polymorph is governed by a combination of intrinsic lattice energy and extrinsic environmental factors such as temperature, pressure, pH, and chemical composition of the surrounding solution. Calcite is widely recognized as the most thermodynamically stable polymorph under ambient conditions [16]. Its low solubility and high resistance to dissolution explain why it occurs in long-term geological processes [174]. The stability of aragonite is profoundly influenced by environmental conditions (T, pH) and the presence of magnesium or strontium (e.g., ionic strength) [175,176]. Furthermore, in alkaline (above pH = 8.3) conditions, aragonite is more likely to form and persist, whereas a low pH (most typically below pH = 7.5) can promote its dissolution and transformation to calcite [177]. Vaterite transformation to calcite was observed to be faster than aragonite crystallization to calcite. Once the local environment, such as pH or temperature, changes, the disordered structure of vaterite can quickly reorganize into calcite [178].

In contrast, the calcium carbonate solvatomorphs, including ikaite and ACC, were mostly observed only transiently during rapid precipitation or biomineralization, and they eventually transform into the more stable calcite or aragonite forms [110]. Monohydrocalcite exhibits intermediate stability, and its formation is favoured under conditions of moder-

ate saturation and in environments with elevated magnesium-to-calcium ratios, where the structural water in the lattice stabilizes it relative to the anhydrous calcite [179]. The transformation from ikaite to calcite involves a substantial loss of crystalline water and occurs via ACC (Lázár et al. [72]). This dehydration process is accompanied by significant changes in the vibrational spectra, as captured by IR and Raman measurements, and has been modelled extensively using both experimental kinetics and theoretical approaches [180]. Synthetic conditions strongly influence the morphology of calcium carbonate polymorphs and solvatomorphs. For instance, Sand et al. found that not only the purity of ethanol used, but agitation of the solution (gentle or vigorous) influenced the shape of the crystalline products. In the following subsection, we review the possible transformation routes of each hydrated $CaCO_3$ and their mutual transformation (Figure 7).

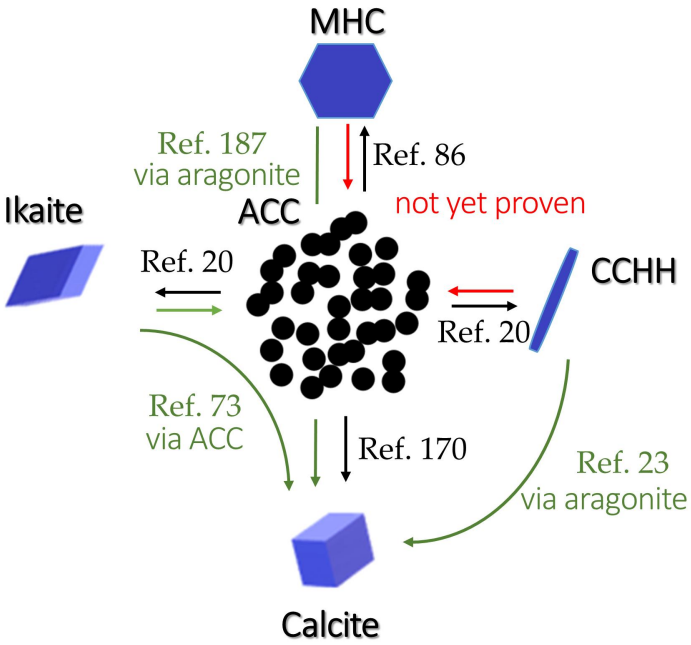


Figure 7. The possible transformation routes of each hydrated $CaCO_3$ and their mutual transformation. The final transformation product for each case is calcite, which is the most stable form of $CaCO_3$ at ambient conditions.

4.1. Transformation of Ikaite

Ikaite is stable only under low-temperature or high-pressure conditions (~300 MPa) [21,73,181–183]. Johnston et al. found that it slowly decomposed at and above 0°C in different organic liquids (diethyl ether, benzene) and transformed into calcite within two days.

Lázár et al. [72] reported that the preparation conditions, such as pH, temperature, Mg-content, and the media, e.g., air or solution, strongly influenced the transformation time and the structure of the final carbonate. For example, ikaite prepared at pH 10.3 and placed on a glass slide was stable for several weeks at 20 °C, whereas it quickly (within 4 h) transformed calcite or vaterite in solution. In clove oil, it was stable for months if the crystals were kept separately [58]. Slight warming led to rapid dehydration and transformation into calcite, often preserving the original crystal morphology in a pseudomorph calcite phase known as glendonite, which could be used to infer cold paleoclimate conditions [73,183].

Ikaite typically forms below 7 °C in sediments [114] and is generally prepared between 0 and 10 °C by direct reaction of carbon dioxide and calcium oxide or calcium carbonate solutions/suspensions [21]. Tollefsen et al. found that ikaite was formed even at 35 °C when pH was between 9.3 and 10.3, and the starting materials were a mixture of natural seawater and sodium carbonate-rich solution [69]. The kinetics of the ikaite transformation have been the subject of many studies, employing both laboratory experiments and field

observations in polar and deep-sea environments. Purgstaller et al. studied the formation and transformation of ikaite in various pH, T, and Ca^{2+} to Mg^{2+} ratios [184]. Strohm et al. studied how phosphate could influence the growth of ikaite crystals [185]. Brečević et al. found the solubility of ikaite ($-\log K_s^\circ$) at 25 °C was 7.1199 [16], which is higher than the previously determined value (6.62) by Clarkson et al. [186]. Lázár et al. [72] reported that ikaite transformation in solution and in air occurs via ACC. Magnesium has a stabilizing effect on ikaite, which is similar to what was found for other hydrated calcium carbonates (MHC and CCHH) [187]. The transformation routes between the calcium carbonate polymorphs and solvatomorphs are complex and influenced by both kinetic and thermodynamic factors. In many natural systems, ACC is an initial transient phase deposited quickly under supersaturated conditions. Over time, ACC transforms into crystalline phases such as vaterite or directly into calcite, depending on the presence of inhibitors (such as organic macromolecules or specific ions) and the prevailing environmental conditions. Tang et al. [188] and Shaikh et al. [189] showed that ikaite can transform into vaterite, and Lázár et al. [21] reported the occurrence of two ACC types that differ in their mode of formation, morphology, particle size, water content, and stability, and found that ikaite formation starts with ACC (I) and ikaite transforms to calcite via ACC (II).

Ikaite transforms into vaterite and calcite at room temperature [189] during heating [136,186,188], or upon dropping it into boiling water [75,105]. Lázár et al. [72] demonstrated that ikaite can also transform into aragonite if the ikaite parent solution contains some Mg^{2+} (26 mg/L) and found that ikaite transforms into calcite via the nanosized ACC (I). However, micron–sized ACC (II) forms if ikaite is treated with polar organic solvents (MeOH, abs. EtOH, n-propanol, and DMSO) [21] and during vacuum pumping at room temperature. ACC (I) is spherical and contains 1.12 mol adsorbed and 0.26 mol chemically bonded water, whereas ACC (II) preserves the morphology of ikaite and is characterized by 0.42 mol absorbed and 0.35 mol chemically bonded water [21].

Sekkal studied different models (Raiteri's and Xiao's) of the surface stabilities of ikaite and found that (001) was the most stable surface with 0.2 J/m^2 surface energy and −2.57 eV attachment energy, which is lower than the (10–14) surface energy of calcite (0.51 J/m^2 and −8.69 eV) [28]. In contrast, (100) and (010) surfaces of ikaite were found to be 0.52 J/m^2 and −8.19 eV, and 0.37 J/m^2 and −5.79 eV values, respectively [28].

4.2. Transformation of MHC

The thermodynamic data of MHC were determined by Hull et al. Its free energy of formation (ΔG_f°) and the standard enthalpy of formation (ΔH_f°) were found to be -325.430 ± 270 cal mol^{-1} and -358.100 ± 280 cal mol^{-1} [190], respectively. Its solubility product ($-\log(K_s^\circ)$ was reported as 7.60 ± 0.03 [190]. However, according to Brečević et al. [16], it is 7.050 ± 0.029 at 15 °C. Krajel et al. [90] found that the different accompanying ions influenced its solubility; the lgK values changed from 7.1772 to 7.4890 on increasing the temperature from 25 °C to 50 °C [90]. Liu et al. showed that the MHC (prepared from artificial seawater), in the absence of any additives, transforms into aragonite over 72 h in solution, even at 4 °C, and then to calcite at the end [191].

The structure of MHC can be stabilized by the presence of Mg^{2+} ions [87,192,193], polymeric substrates like sulfonated polystyrene and polystyrene-divinylbenzene [194], oxalate ions [195], or silica-rich environments [89,196]. Rodriguez-Blanco et al. studied the effect of the Ca^{2+} to Mg^{2+} ratio in aqueous solutions between 65 and 0.17 [87], and found that the magnesium ions inhibited calcite formation [197,198].

Based on PXRD measurements, Rodriguez-Blanco et al. [87] reported that magnesium-containing ACC (ACMC) was stable for 8 h and transformed into MHC in 10 h (Figure 8). Von Euw et al. followed the transformation of ACMC into MHC with solid-state NMR

and found that 40% of the carbonate ions of ACMC converted into MHC after 20 h [199]. Ghilardi et al. found that marine species, such as coral reef fishes, mostly produced MHC and ACMC; however, their ratio was species dependent [13].

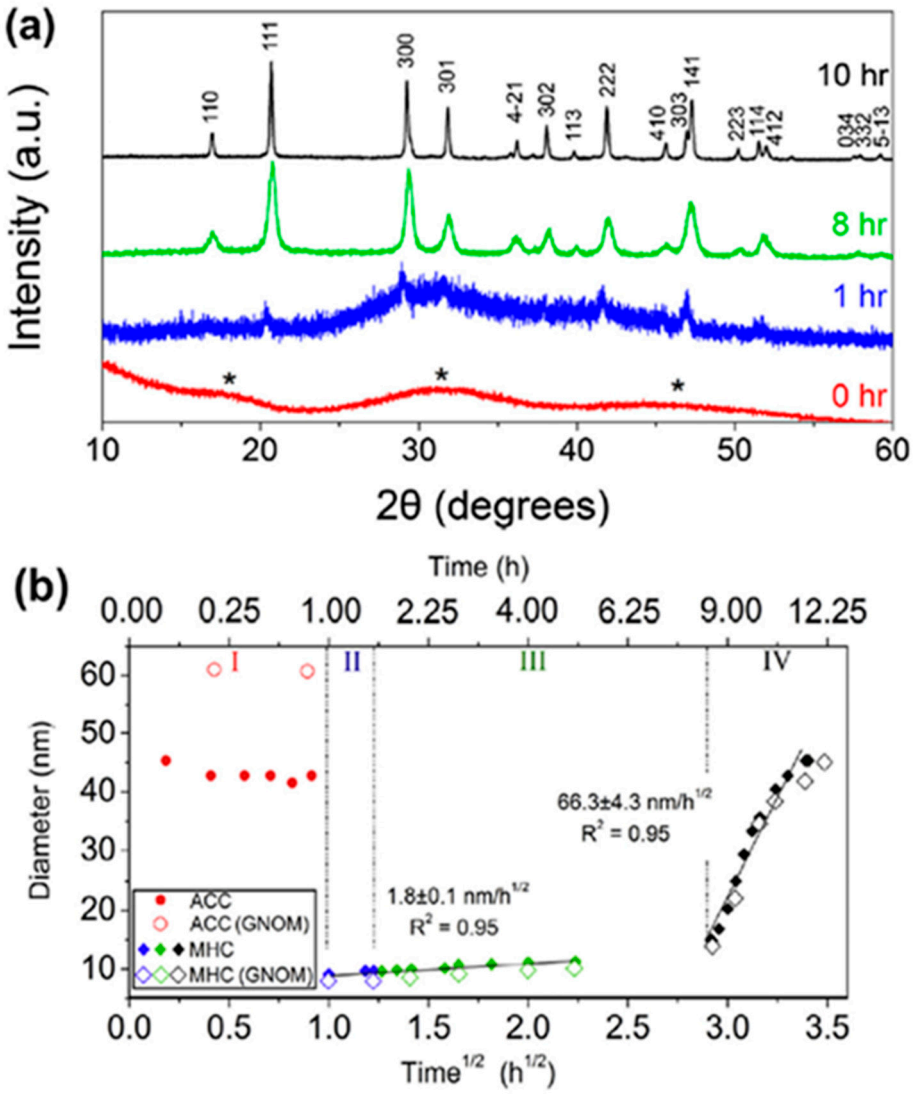


Figure 8. The transformation of ACC into MHC, followed by PXRD (**a**), and the time evolution of the particle diameters for the initial amorphous phase (**b**). Reproduced from Rodriguez-Blanco et al. [87]. Please note that the "*" represent the amorphous phase.

Korneva et al. [141] and Kimura et al. [200] followed the thermal transformations of synthetic MHC by TG/DTA-MS, PXRD, and FT-IR [200], and the kinetic parameters of the thermal dehydration were determined [200]. Heating of MHC at 443 K for 60 min resulted in the growth of calcite peaks in PXRD [200]. The thermal dehydration-initiated calcite nucleation on the MHC particle surfaces was characterized by a distinguished induction period and self-induced gelation with E_{ip} = 228.1 ± 8.6 kJ mol^{-1} and E_a = 210.3 ± 5.1 kJ mol^{-1}, respectively. As it was mentioned in Section 2, Kimura et al. showed two different MHC morphologies, spherical and spherical polygons (Figure 1C), and twisted spindles (Figure 1D) were formed at 288 and 303 K, respectively. They characterized the two kinds of grains with TG-DTA-MS, and two distinct curves were found (Figure 9A and B, respectively). The sample, prepared at 288 K, started to lose water at 432 K and decomposed between 460 and 485 K with calcite formation [74]. In contrast, the sample, prepared at

303 K, decomposed in a wide temperature range (400–560 K), and its PXRD data showed no diffraction peak up to 523 K, consistent with the decomposition product of ACC [74].

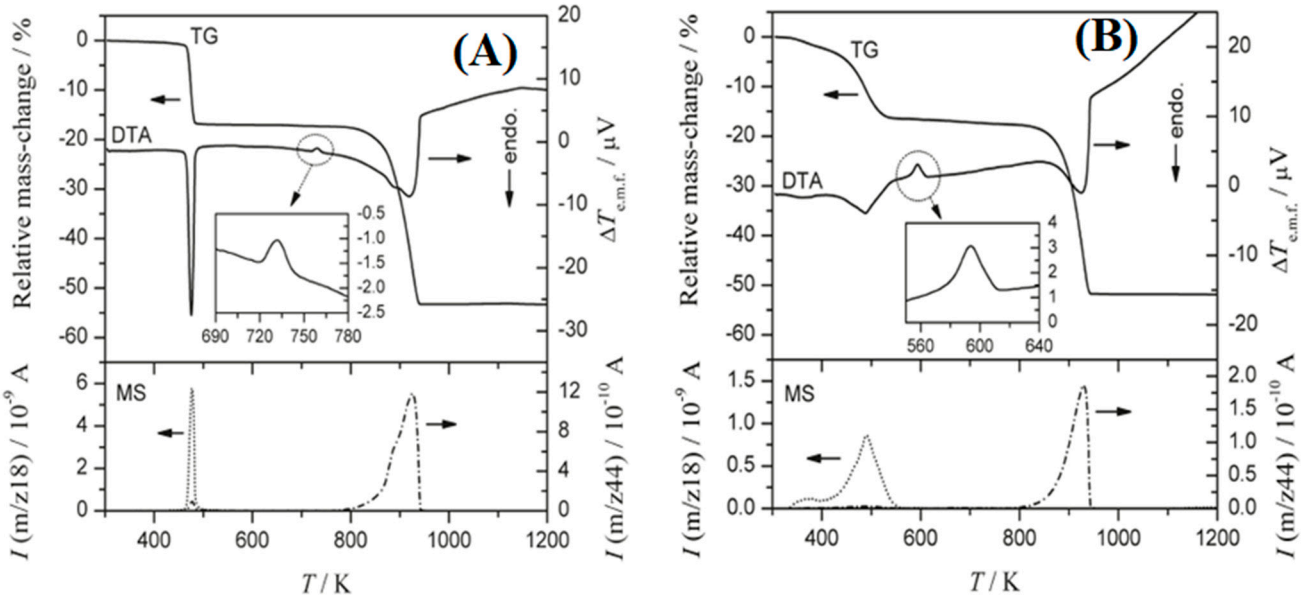


Figure 9. (**A**,**B**) panels show the TG-DTA-MS curves of two MHC grains with distinct morphology, prepared in 20 mol% Mg-containing mother liquor at 288 K and 303 K, respectively. Reproduced from the work of Kimura et al. [74] with permission.

Zhang et al. studied how silica-gel media could influence the morphology of MHC [89,196] between 25 and 70 °C (Figure 10) [201]. The MHC nanoparticles, formed upon mixing the starting solutions, were self-aggregated into nanorods and spontaneously self-organized into particles with distinct morphology depending on temperature, which can be explained by, e.g., the dipole–dipole interactions [201].

Chaka et al. performed DFT calculations [187] to determine the effect of Mg^{2+} and H_2O contents during the formation of MHC. They found that the Mg atom had a higher water binding energy than Ca^{2+}, which promoted the formation of MHC. However, the thermodynamic stability of MHC decreased due to the presence of a small amount of Mg (11.1 mol%), which resulted in a structural distortion. This destabilizing effect was enhanced if the CO_2 pressure was increased from 1 to 90 bar [187]. Sekkal et al. determined that the most stable surface of the MCH by the DFT method was (001) with 0.99 J/m^2 surface energy and −5.66 eV attachment energy, which was higher than the most stable (10–14) surface of calcite [28]. The (100) and (010) surfaces of MHC ((100) and (010)) were determined to be 1.54 J/m^2 with −7.82 eV and 1.21 J/m^2 with −6.62 eV, respectively [28].

4.3. Transformation of Various ACCs

Synthesis of ACC was recently reviewed by Jiang et al. [24]. Pure ACC is metastable, typically lasting from a few minutes to several hours. However, the presence of magnesium or phosphate ions, or organic macromolecules, can enhance its stability, significantly extending its lifetime. Additionally, factors such as pH play a crucial role by influencing the structure and properties of ACC through the carbonate/bicarbonate equilibrium and the availability of hydroxyl groups [25,29,202–205]. Furthermore, water has a significant influence on the stability and transformation routes of the ACC [206]. Recently, Maslyk et al. presented a study that describes a way to prepare an intermediate phase, which was proved to be an amorphous calcium carbonate monohydrate (aMHC) that was suggested by the combination of PXRD, FT-IR, and solid-state NMR [206].

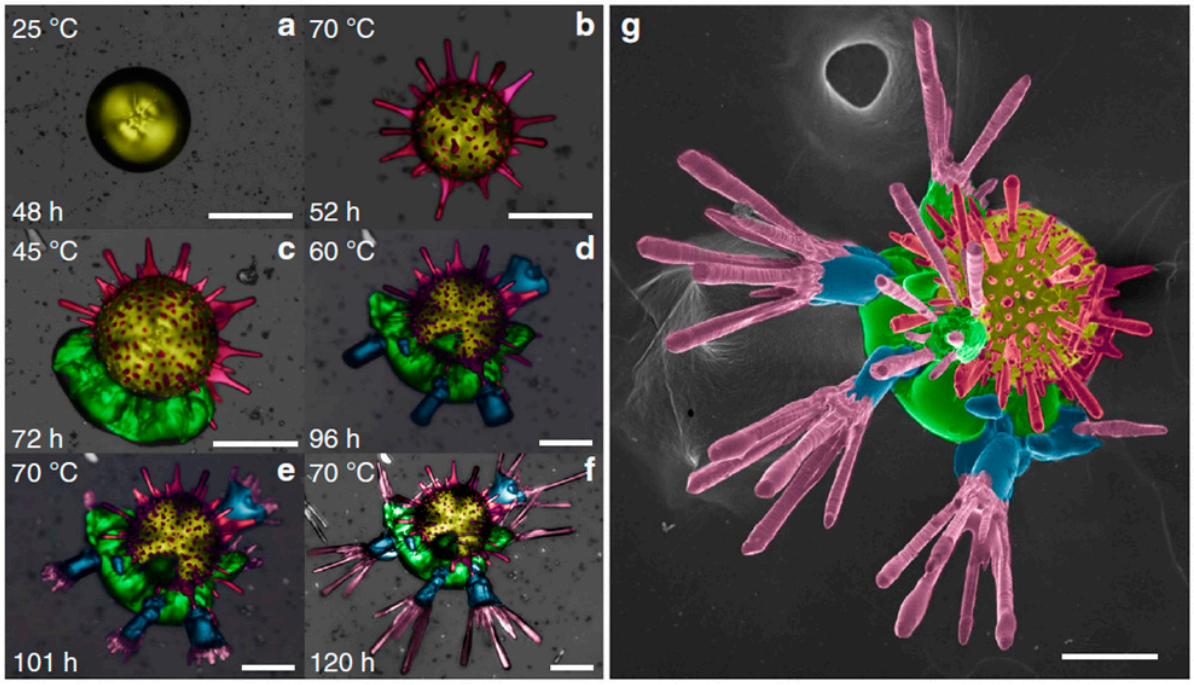


Figure 10. Optical micrographs (**a**–**f**) and the coloured FESEM image (**g**) (scale bar: 100 μm in both cases) demonstrate that temperature and crystallization time influence the structure of the as-grown MHC. Growth history of multi-textured complex architectures of MHC. The growth periods at different temperatures and times: 25 °C (0–48 h), 70 °C (48–52 h), 45 °C (52–72 h), 60 °C (72–96 h), and again 70 °C (96–120 h). The different colours represent the different periods. Reproduced from the work of Zhang et al. [201] with permission.

In addition to the stabilization effect of the phosphate ion [202,204], some biological entities produce different solvatomorphs of $CaCO_3$, including ACC, which is the so-called biogenic ACC [109]. Furthermore, these biogenic products were found to be more stable than those without any organic stabilizer. The same stabilization effects of different polymer and organic materials were reported [44,207–211], For example, Yasue et al. used PEG (in ethanol) during the production of ACC [212]. Laboratory experiments unambiguously showed that the transformation of ACC occurs by dissolution–reprecipitation mechanisms, in which local restructuring and water reorganization lead to the nucleation of a more stable phase. Similar pathways were observed in biomineralization, and organisms control the phase transformation by modulating the local chemical environment and by secreting organic matrices that stabilize ACC until crystal nucleation is triggered.

Various synthetic reaction routes yielded ACCs with distinct water contents. Radha et al. determined that the H_2O content of the synthetic and the biogenic ACC were between 1.20 and 1.58 moles and 0.16 to 0.35 moles per formula unit, respectively [12]. They found that the dehydration of ACC had an exothermic nature, which means that irreversible structural reorganization occurred during the dehydration reaction. The measured enthalpy of the crystallization at ambient conditions for the synthetic and biogenic ACC samples was found to be from -17 ± 1 to -24 ± 1 kJ/mol and -14.3 ± 0.97 kJ/mol, respectively. Synthetic ACCs were less ordered and more metastable than the biogenic ACCs [12]. Brečević et al. [16] and Purgstaller et al. [205] determined the solubility of ACC with about 0.5 mol of crystalline water as logK = -6.1987 and -6.20 ± 0.02 [205], respectively. Purgstaller et al. found that the log$K$ value was changed to -4.42 ± 0.01 as a result of amorphous magnesium carbonate (AMC) formation. They investigated the effect of different magnesium ion content and determined the stability and v_1 mode position in Raman spectra (Table 4) [205].

Table 4. The summary of the effect of the Mg^{2+} ion content on the position of υ_1 (Raman shift), stability, and solubility of the ACC [205].

Sample Composition	υ_1 (Raman Shift)	Stability in Solution (Min)	logK
ACC	1080 ± 1	15	−6.20 ± 0.02
$\mathbf{Ca_{0.91}Mg_{0.09}}$	1082 ± 1	24	−6.13 ± 0.02
$\mathbf{Ca_{0.85}Mg_{0.15}}$	1082 ± 1	24	−6.13 ± 0.02
$\mathbf{Ca_{0.78}Mg_{0.22}}$	1083 ± 1	54	−6.04 ± 0.03
$\mathbf{Ca_{0.69}Mg_{0.31}}$	1084 ± 1	85	−6.00 ± 0.03
$\mathbf{Ca_{0.61}Mg_{0.39}}$	1085 ± 1	64	−5.81 ± 0.07
$\mathbf{Ca_{0.47}Mg_{0.53}}$	1086 ± 1	51	−5.71 ± 0.03
$\mathbf{Ca_{0.20}Mg_{0.80}}$	1088 ± 1	20	−5.43 ± 0.02
AMC	1095 ± 1	9	−4.96 ± 0.01

Radha et al. showed that although the difference in the amount of crystalline water in ACC did not influence the XRD positions of the amorphous humps centred at 20 and 45° 2Θ, the intensity ratio of the IR active υ_2 to υ_4 modes changed from around 9.5 to around 6.2 if less crystalline water occurred in the structure [12]. Ihli et al. studied the dehydration and crystallization of ACC in solution and in air with TGA, DSC, SEM, NMR, and IR spectroscopy and developed a model for the ACC to calcite crystallization Figure 11a–e [213].

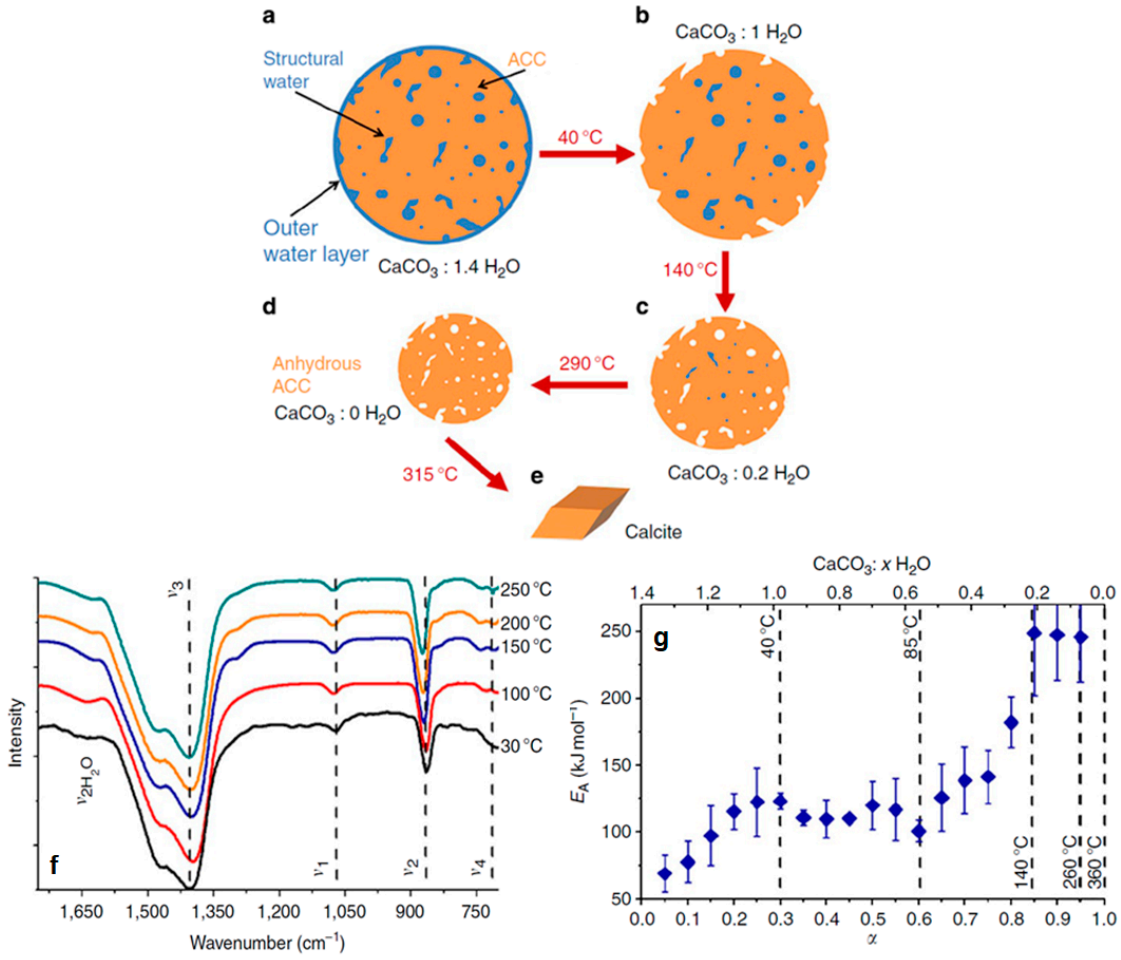


Figure 11. ACC dehydration and transformation (in solid-phase) (**a**–**e**). The evolution of the ACC IR spectra and activation energies during heat treatment and dehydration (**f**). The summary of the activation energies of the dehydration of ACC (**g**). Reproduced from Ihli et al. [213] with permission.

The overall ACC dehydration process is accompanied by a structural rearrangement, which resulted in a sharpening of the υ_3 IR band, reducing the intensity υ_1 IR peak, and a slight shifting in the υ_2 IR band positions toward higher frequencies (Figure 11f). However, the DSC results did not show any crystallization process up to 290 °C [213]. The activation energies (E_a) of the different dehydration steps are summarized in Figure 11g, which shows a general increase in the E_a values with increasing dehydration. Three well-separated dehydration steps (Figure 11g) are attributed to the presence of three different amounts of H_2O (noted with x) in ACC (Figure 11, where (a): $x = 1.4 - 0.98$ and $E_a = 80$ kJ/mol, (b): $x = 0.98 - 0.25$ and $E_a = 145$ kJ/mol, and (c): $x = 0.25 - 0.08$ and $E_a = 245$ kJ/mol [213]). According to Ihili et al., ACC fully transforms into calcite above 290 °C, a bit lower temperature than that found by Radha et al. [12] or Reeder et al. [213] (330–340 and 290–400 °C, respectively), with E_a 125 J/mol.

ACC, prepared without any additives, is commonly reported to be stable only for minutes to 4 days at ambient temperature and atmosphere, and after this period, it transforms into crystalline $CaCO_3$ [214,215]. The alternative crystallization pathways of ACC, which involve stable clusters, were reviewed by Gebauer et al. [216]. Rodriguez-Blao et al. studied the ACC transformation into calcite via vaterite at 7.5 °C in air with the Energy Dispersive X-ray diffraction (EDXRD) technique and identified two transformation stages: *Stage I*, representing the ACC → ACC + vaterite → vaterite crystallization, which took 14–45 min, and *Stage II*, representing the vaterite → vaterite +calcite → calcite recrystallization, which took about 18 h. The increase in temperature up to 25 °C increased the velocity of transformation to 12 min and 3 h, respectively [180]. It is of interest that Besselink et al. identified a "short-lived" ikaite formation before *Stage I*, which was facilitated by the low temperature conditions and the presence of chelating citrate ligands [167]. Bots et al. followed the transformation of ACC with small- and wide-angle X-ray scattering (SAXS/WAXS) and identified three stages, including the following: (I) the dehydration of hydrated and disordered ACC, which did not show Bragg peaks and occurred 60s to 90s after the mixing; (II) the transformation of ordered ACC to vaterite, evidenced by X-ray background decrease, and the occurrence of weak vaterite peaks about 4–6 min after mixing and their increase 35 min after the mixing; and (III) the formation of calcite (Figure 12A) [217]. The SEM pictures showed that the 30–40 nm-sized ACC spheres aggregated and transformed into micron-sized vaterite (Figure 12B–D) [217]. An identical morphological transformation was found by Galan et al. [41] and Cai et al. [218].

Studying ikaite formation and its recrystallization, Lázár et al. recognized two morphologically and chemically distinct ACCs [21]. They identified ACC (I), which occurred below 5 °C as 50–100 nm-sized spheres, contained 1.12 mol absorbed and 0.26 mol chemically bonded water, and transformed to ikaite within 10–25 min, and ACC(II), which was micron-sized and preserved the morphology of ikaite, contained 0.42 mol absorbed and 0.35 mol chemically bonded water, and slowly (within hours) transformed to calcite [21]. ACC (I) could be dehydrated to 0.03 mol water upon heating and before its transformation to calcite at 300 °C in air, whereas for ACC(II), calcite transformation was temperature dependent and took more than 24 h at 75 °C and 10–30 min at 150 °C [21]. Interestingly, Lázár et al. [72] reported that ACC (I) occurs during the ikaite-to-calcite transformation, also, and not only as a precursor phase before ikaite formation. In the presence of strontium ions, vaterite did not occur as a transient phase, but the anhydrous ACC immediately transformed into calcite [172]. However, based on Raman studies, Molnár et al. [173] reported the formation of an aragonite-type structure from increased Sr-containing ACC.

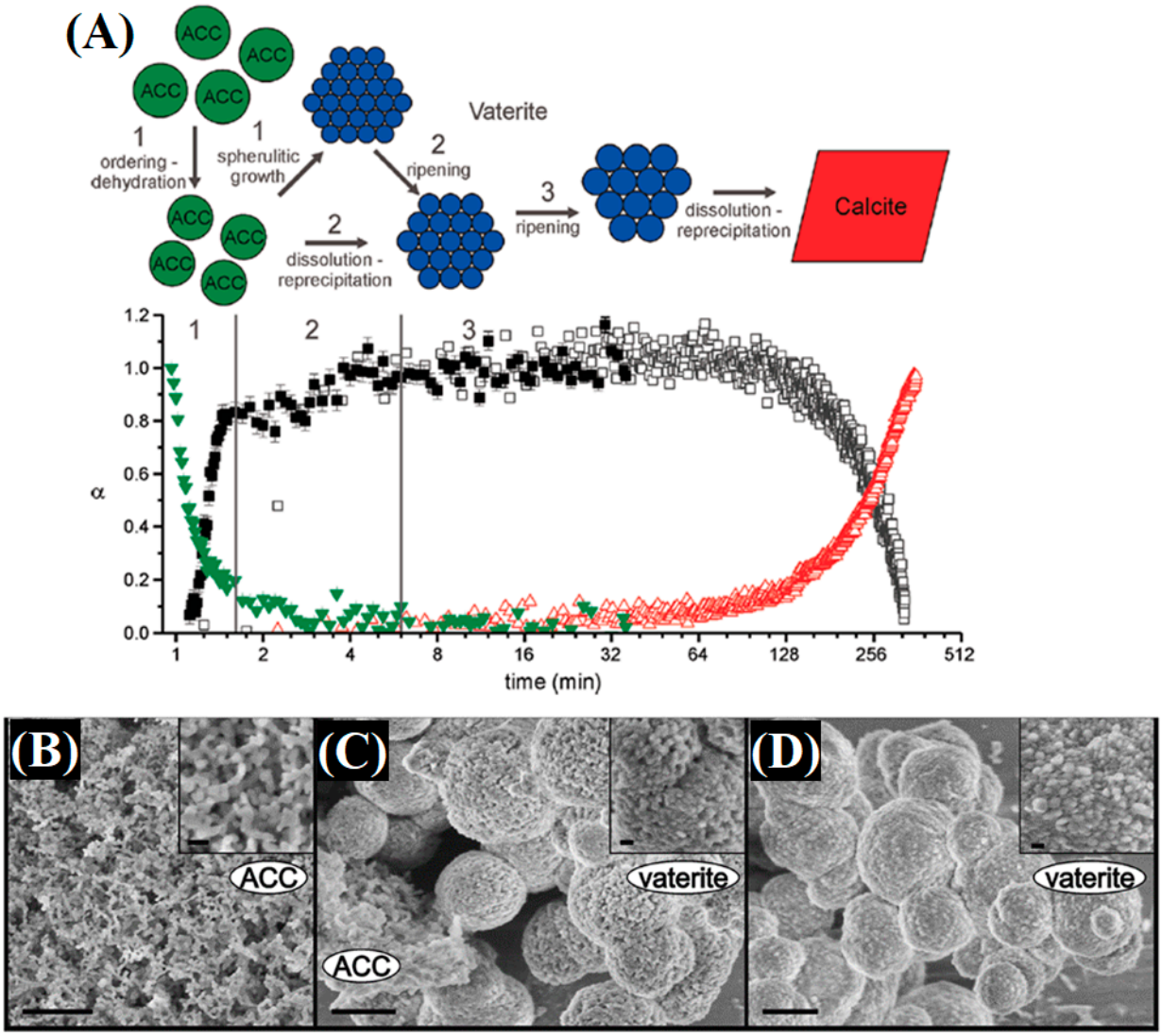


Figure 12. The schematic representation of the multistage ACC → vaterite → calcite crystallization pathway. (**A**) Transformation of ACC into vaterite 1 min (**B**), 2 min (**C**), and 35 min (**D**) after the mixing. Scale bars are 100 nm in (**B**–**D**). Reproduced from Bots et al. [217] with permission. The green triangles and full black squares represent the ACC and vaterite from Bots et al. [217] study, and the open squares and red triangles represent the vaterite and calcite from Rodriguez-Blanco et al. [180].

Konrad et al. studied ACC stability and the effect of freeze-drying to remove physiosorbed surface water by PXRD, in situ Raman, SEM, and TEM methods [131]. They reported that gastight sealing could stabilize ACC even up to 150 days, and ACC started to transform into anhydrous polymorphs of $CaCO_3$ after 51 days in a semi-tight container (Figure 13B), but there was some ACC leftover even after 87 days [131]. In an open container, only 5 days of stability could be reached (Figure 13A). Freeze-drying by itself did not have a significant effect on the stability of the ACC [131].

Galan et al. studied the transformation of ACC in solution in the presence of vaterite with and without $MgCl_2$ additive up to 120 h [41]. The presence of vaterite accelerated the ACC transformation reactions and the calcite formation, whereas the presence of Mg^{2+} inhibited vaterite precipitation at the early stages and promoted the direct transformation of ACC into calcite [41] (Figure 14).

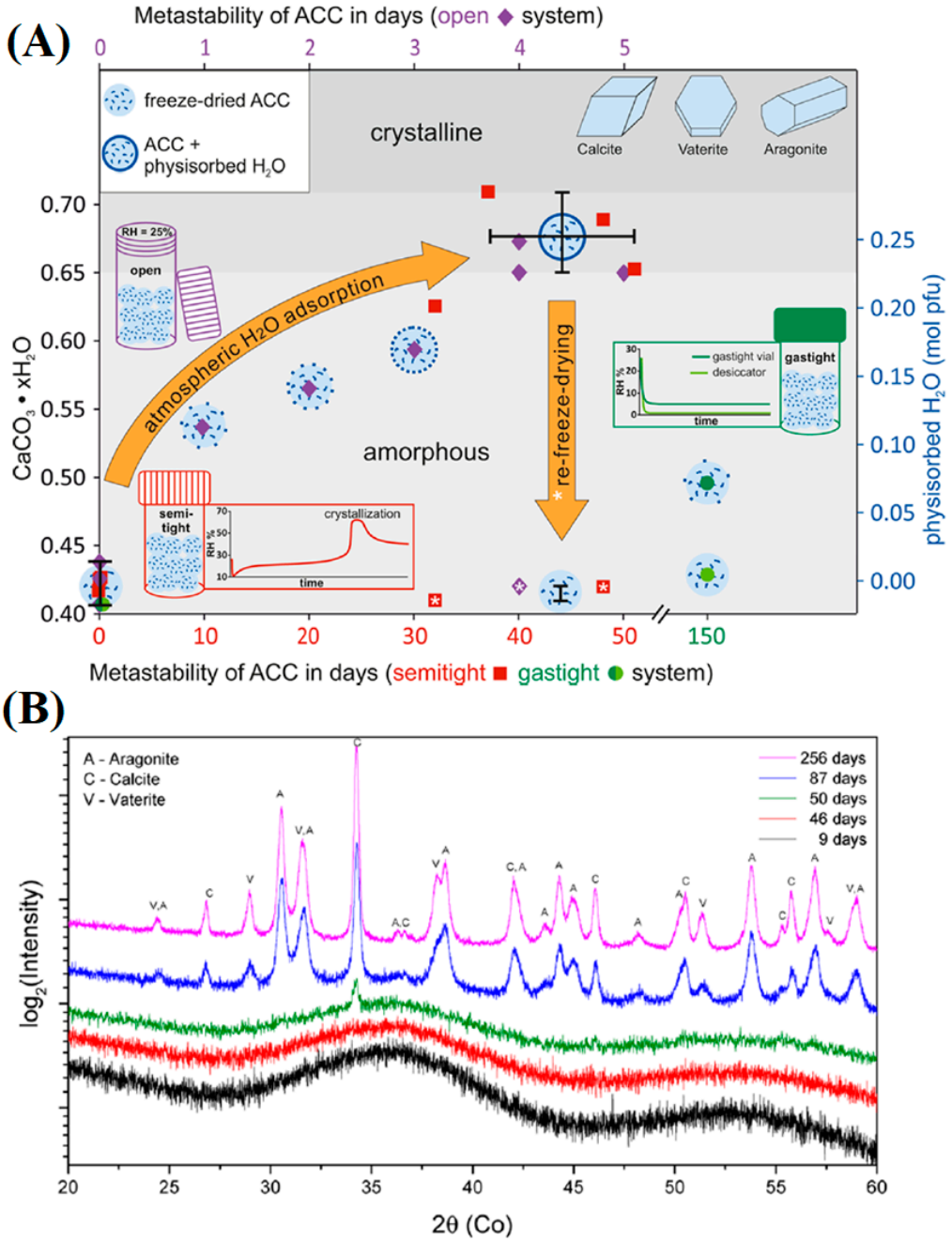


Figure 13. Schematic diagram illustrating the H_2O physisorption process by plotting measured H_2O contents of ACC vs. observed ACC metastability (**A**) and the PXRD patterns of the semi-tight ACC samples as a function of time (**B**). Reproduced from Konrad et al. [131] with permission (RH% = relative humidity).

4.4. Transformation of CCHH

The last known member of the $CaCO_3$ solvatomorph series is the CCHH, which is stabilized by Mg^{2+} ions and prepared from a premixed solution of $CaCl_2$ and $MgCl_2$ by adding Na_2CO_3 after the immediately precipitated, 6.5% Mg-containing ACC [20]. The chemical composition of the amorphous phase was found to be $Ca_{0.98}Mg_{0.02}CO_3 \cdot xH_2O$, where x = 0.48. It transformed into a new needle-like, ~ 200 nm diameter and 1–5 mm long crystalline material in ~1 h. The transformation was marked by a sharp decrease in Ca^{2+} activity in the solution and was accompanied by an increase in pH, suggesting a mechanism in which Mg^{2+} ions were being excluded from the growing crystals. The initial solution contained Mg^{2+} at high concentration, whereas the final CCHH phase

contained only about 1.5 *n*% Mg [20]. When the concentrations of $CaCl_2$, $MgCl_2$, and Na_2CO_3 were selected to be 0.05, 0.06, and 0.05 mol/kg, respectively, the CCHH formed from ACC after 60–110 min and was found to be stable over 5 h (Figure 15E–H) [23]. The Ca^{2+} concentration decreased while the Mg^{2+} concentration was set back to almost the initial concentration, and pH increased when CCHH crystallization started. The Mg^{2+} ions were released during the transformation, and only about 3–4% Mg^{2+} was left in the CCHH (Figure 15H) [23]. When the aragonite peaks appeared on the diffractograms (and, therefore, in the system) after 400 min, the pH, alkalinity, and Ca^{2+} concentration suddenly decreased in the solution (Figure 15E) [23], which agrees well with the findings of Zou et al. [20] and a kinetic control by magnesium. Mg^{2+} ions hindered the complete dehydration of ACC, thus maintaining a partial level of hydration in the final crystalline product [20]. Suyama et al. determined its solubility (logK = -6.80 ± 0.05) and its thermodynamic properties: $\Delta G_f^\circ = -1238.2 \pm 0.3$ kJ/mol [23]. Comparing the standard free enthalpies of formation for hydrated $CaCO_3$ solvatomorphs, the thermodynamic stability order was found to be as follows: ACC < ikaite < CCH < MHC < vaterite < aragonite < calcite, which agrees well with the transformation line ACC → CCHH → Aragonite → Calcite [23]. The thermodynamic modelling and experimental decomposition results of CCHH showed that this solvatomorph is stable only within a narrow window of humidity and temperature, generally between 10 and 30 °C, and at intermediate relative humidities. Outside these conditions, CCHH tends to dehydrate into calcite, or, under high humidity, it may hydrate further into monohydrocalcite. CCHH is sensitive to both drying and heating, decomposing by releasing its bound water and transforming into anhydrous crystalline form. As a result, the CCHH only appeared in specific micro-environments in nature, such as magnesium-rich sediments [20], but its formation was predicted during evaporation in highly alkaline natural lakes [23].

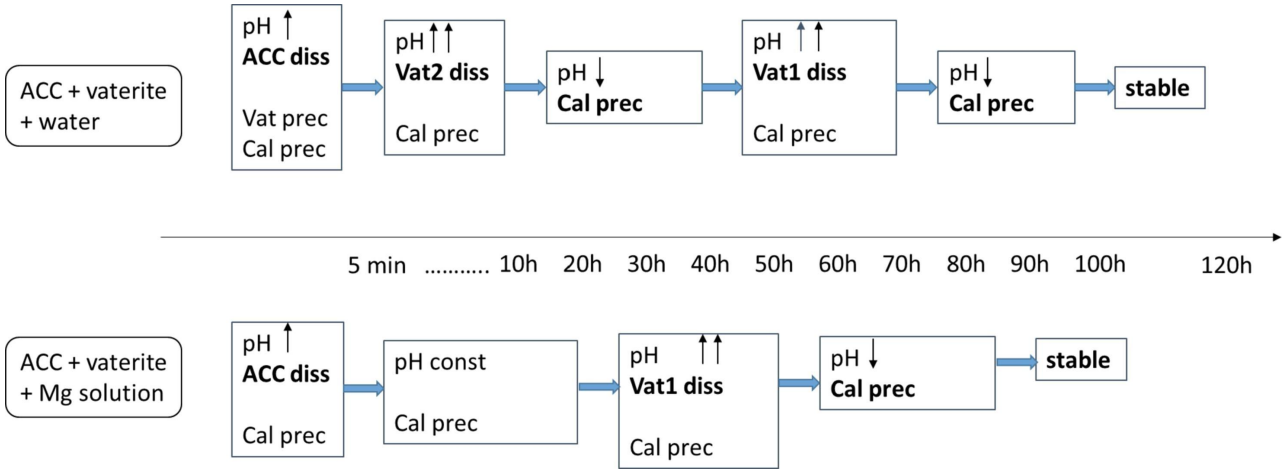


Figure 14. Schematic representation of the transformation processes of ACC in water and $MgCl_2$ solution. **Vat1** and **Vat2** are initially occurring vaterite and the product formed during the transformation of ACC, respectively. The dominant process at each stage is marked in bold. Reproduced from Galan et al. [41] with permission.

The biomineralization of MHC and CCHH was followed by Schmidt et al. in different natural materials (e.g., coral skeleton) with Myriad Mapping (MM) and FT, and Synchrotron Infrared Nano Spectroscopy (SINS) [22]. A multi-step route was found; the main difference was that aragonite could be formed in many different ways, but calcite formed in two ways only (Figure 15A–D). The same transformation route of CCHH was detected by PXRD [23]. After 370 min of the CCHH synthesis, aragonite appeared and became the dominant phase

with calcite after about 430–480 min [22]. The pH, Ca, or Mg concentration was reported to influence these transformations (Figure 15E,H).

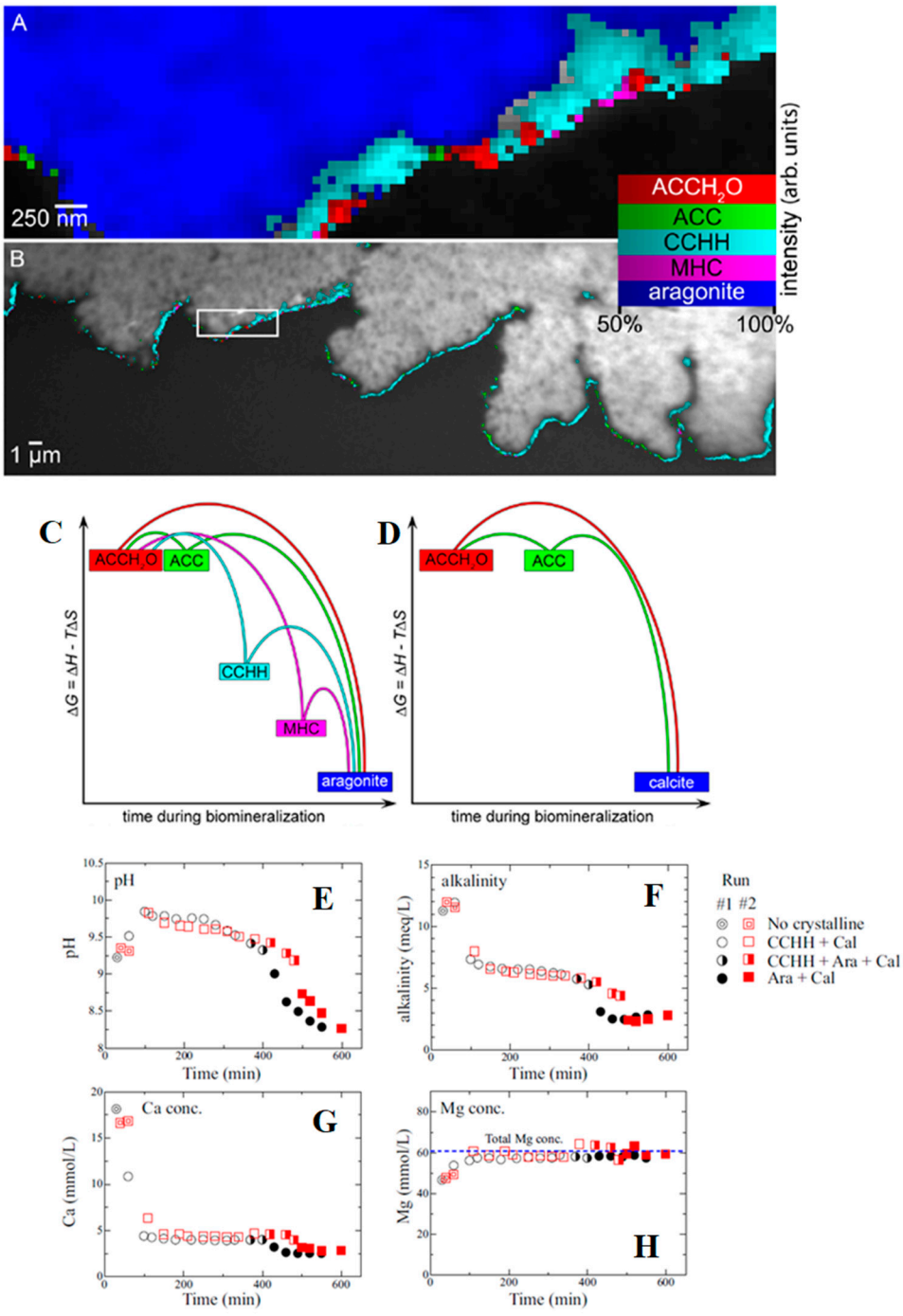


Figure 15. The Myriad Mapping (MM) (**A**,**B**) and the biomineralization routes (**C**,**D**) of the MHC and CCHH and the transformation of CCHH. (**C**) shows four pathways to crystallization from ACC·H_2O to a mature aragonite biomineral: direct or through ACC only, the other two pathways include, one at a time, CCHH or MHC, whereas (**D**) shows only two pathways from ACC·H_2O to a mature calcite biomineral, either directly or through ACC. (**E**) pH, (**F**) alkalinity, (**G**) Ca concentration, and (**H**) Mg concentration as functions of reaction time. Figure (**A**–**D**) are reproduced from the work of Schmidt et al. [22], whereas (**E**–**H**) from Suyama et al. [23].

5. Conclusions and Future Perspectives

Ikaite, MHC, CCHH, and ACC are hydrated calcium carbonates and represent a complex and dynamic group of solvatomorphs, characterized by distinct morphologies and structural, chemical, and thermodynamic properties. Despite their relatively simple chemical compositions, these phases exhibit unique hydration states, coordination environments, transformation pathways, and environmental stabilities. Recent advances in characterization techniques—such as IR, Raman, and NMR spectroscopies, PXRD, and EXAFS—DFT and MD computational modelling, and in situ monitoring have significantly enhanced our understanding of the formation mechanisms, stability, and mutual interconversions of $CaCO_3$ solvatomorphs. The discovery of CCHH and the identification of distinct ACC forms, such as ACC I and ACC II, have highlighted the complex influence of water content, hydrogen bonding, and environmental conditions on the structure–property relationships within the hydrated $CaCO_3$ system. The role of these hydrated phases as precursors in biomineralization, along with their transient occurrence in cold or chemically specific environments, highlights their significance in both biological and geological contexts. Moreover, the transformation of ACC and related precursors into more stable crystalline polymorphs, such as calcite and aragonite, proceeds through kinetically sensitive pathways, governed by factors including temperature, pH, Mg^{2+}/Sr^{2+} content, and the presence of organic additives. The metastability of ACC, its intermediate role, and its capacity to incorporate foreign ions make it a particularly compelling target for ongoing research in the fields of biomineralization and climate proxy development.

Advancing our understanding of hydrated calcium carbonate phases will require sustained interdisciplinary research that integrates crystallography, spectroscopy, geochemistry, and computational chemistry—bridging natural and engineered systems alike.

Author Contributions: Conceptualization, L.K. and K.A.B.; writing—original draft preparation, K.A.B. and L.K.; writing—review and editing, L.K. and P.N.; visualization, K.A.B.; supervision, L.K. and P.N. All authors have read and agreed to the published version of the manuscript.

Funding: This research was supported by the Grant No. ANN 141894 and Grant No. RRF-2.3.1-21-2022-00014 from the NKFIH.

Data Availability Statement: No new data were created or analyzed in this study. Data sharing is not applicable to this article.

Acknowledgments: For the preparation of the Graphical Abstract, the content of the following works was used (with permissions): Lázár et al. [21], DeVol et al. [33], Kimura et al. [74] and Sand et al. [166].

Conflicts of Interest: The authors declare no conflicts of interest.

References

1. Leonard, J.E.; Cameron, B.; Pilkey, O.H.; Friedman, G.M. Evaluation of Cold-Water Carbonates as a Possible Paleoclimatic Indicator. *Sediment. Geol.* **1981**, *28*, 1–28. [CrossRef]
2. Zervas, A.; Stougaard, P.; Thøgersen, M.S. Complete Genome Sequence of "Bacillaceae Sp. Strain IKA-2": A Cold-Active, Amylase-Producing Bacterium from Ikaite Columns in SW Greenland. *Microbiol. Resour. Announc.* **2024**, *13*, e00887-23. [CrossRef]
3. Schmidt, M.; Priemé, A.; Stougaard, P. Bacterial Diversity in Permanently Cold and Alkaline Ikaite Columns from Greenland. *Extremophiles* **2006**, *10*, 551–562. [CrossRef]
4. Chekanov, G.S.; Shelgunov, V.V. Hexahydrate Deposits in Recirculating Systems for Hydraulic Ash Removal and Ways to Eliminate Them. *Elektr. Stantsii* **1991**, *10*, 10–13.
5. Malkaj, P.; Chrissanthopoulos, A.; Dalas, E. The Overgrowth of Calcium Carbonate Hexahydrate on New Functionalized Polymers. *J. Cryst. Growth* **2002**, *242*, 233–238. [CrossRef]
6. Thakur, S.K.; Tomar, N.K.; Pandeya, S.B. Influence of Phosphate on Cadmium Sorption by Calcium Carbonate. *Geoderma* **2006**, *130*, 240–249. [CrossRef]

7. Trzcinski, A.P.; Stuckey, D.C. Inorganic Fouling of an Anaerobic Membrane Bioreactor Treating Leachate from the Organic Fraction of Municipal Solid Waste (OFMSW) and a Polishing Aerobic Membrane Bioreactor. *Bioresour. Technol.* **2016**, *204*, 17–25. [CrossRef]
8. Kaplan, M.E. Calcite Pseudomorphs in Sedimentary Rocks and Their Paleogeographical Significance. *Dokl. Akad. Nauk SSSR* **1977**, *237*, 1467–1470.
9. Suess, E.; Balzer, W.; Hesse, K.-F.; Müller, P.J.; Ungerer, C.A.; Wefer, G. Calcium Carbonate Hexahydrate from Organic-Rich Sediments of the Antarctic Shelf: Precursors of Glendonites. *Science* **1982**, *216*, 1128–1131. [CrossRef] [PubMed]
10. Vasileva, K.; Vereshchagin, O.; Ershova, V.; Rogov, M.; Chernyshova, I.; Vishnevskaya, I.; Okuneva, T.; Pokrovsky, B.; Tuchkova, M.; Saphronova, N.; et al. Marine Diagenesis of Ikaite: Implications from the Isotopic and Geochemical Composition of Glendonites and Host Concretions (Palaeogene–Neogene Sediments, Sakhalin Island). *Sedimentology* **2021**, *68*, 2227–2251. [CrossRef]
11. Politi, Y.; Arad, T.; Klein, E.; Weiner, S.; Addadi, L. Sea Urchin Spine Calcite Forms via a Transient Amorphous Calcium Carbonate Phase. *Science* **2004**, *306*, 1161–1164. [CrossRef]
12. Radha, A.V.; Forbes, T.Z.; Killian, C.E.; Gilbert, P.U.P.A.; Navrotsky, A. Transformation and Crystallization Energetics of Synthetic and Biogenic Amorphous Calcium Carbonate. *Proc. Natl. Acad. Sci. USA* **2010**, *107*, 16438–16443. [CrossRef]
13. Ghilardi, M.; Salter, M.A.; Parravicini, V.; Ferse, S.C.A.; Rixen, T.; Wild, C.; Birkicht, M.; Perry, C.T.; Berry, A.; Wilson, R.W.; et al. Temperature, Species Identity and Morphological Traits Predict Carbonate Excretion and Mineralogy in Tropical Reef Fishes. *Nat. Commun.* **2023**, *14*, 985. [CrossRef]
14. Photong, C.; Pragot, W. Effect of Adding Monohydrocalcite on the Microstructural Change in Cement Hydration. *ACS Omega* **2022**, *7*, 36318–36329. [CrossRef]
15. Lee, S.K.; Oh, T.; Kim, G.W.; Bae, S.; Yoo, D.-Y. Benefits of $CaCO_3$ Nanoparticles for the Strain Hardening Behavior of High-Strength Alkali-Activated Composites Based on Blast Furnace Slag and Liquid Crystal Display Glass Powder. *Constr. Build. Mater.* **2024**, *449*, 138314. [CrossRef]
16. Brečević, L.; Kralj, D. On Calcium Carbonates: From Fundamental Research to Application. *Croat. Chem. Acta* **2007**, *80*, 467–484.
17. Nebel, H.; Neumann, M.; Mayer, C.; Epple, M. On the Structure of Amorphous Calcium Carbonate—A Detailed Study by Solid-State NMR Spectroscopy. *Inorg. Chem.* **2008**, *47*, 7874–7879. [CrossRef] [PubMed]
18. Fischbeck, R.; Müller, G. Monohydrocalcite, Hydromagnesite, Nesquehonite, Dolomite, Aragonite, and Calcite in Speleothems of the Frankische Schweiz, Western Germany. *Contrib. Mineral. Petrol.* **1971**, *33*, 87–92. [CrossRef]
19. Mackenzie, J.E. CCLXXIV.—Calcium Carbonate Hexahydrate. *J. Chem. Soc. Trans.* **1923**, *123*, 2409–2417. [CrossRef]
20. Zou, Z.; Habraken, W.J.E.M.; Matveeva, G.; Jensen, A.C.S.; Bertinetti, L.; Hood, M.A.; Sun, C.; Gilbert, P.U.P.A.; Polishchuk, I.; Pokroy, B.; et al. A Hydrated Crystalline Calcium Carbonate Phase: Calcium Carbonate Hemihydrate. *Science* **2019**, *363*, 396–400. [CrossRef] [PubMed]
21. Lázár, A.; Molnár, Z.; Demény, A.; Kótai, L.; Trif, L.; Béres, K.A.; Bódis, E.; Bortel, G.; Aradi, L.E.; Karlik, M.; et al. Insights into the Amorphous Calcium Carbonate (ACC) → Ikaite → Calcite Transformations. *CrystEngComm* **2023**, *25*, 738–750. [CrossRef]
22. Schmidt, C.A.; Tambutté, E.; Venn, A.A.; Zou, Z.; Castillo Alvarez, C.; Devriendt, L.S.; Bechtel, H.A.; Stifler, C.A.; Anglemyer, S.; Breit, C.P.; et al. Myriad Mapping of Nanoscale Minerals Reveals Calcium Carbonate Hemihydrate in Forming Nacre and Coral Biominerals. *Nat. Commun.* **2024**, *15*, 1812. [CrossRef]
23. Suyama, M.; Kitajima, T.; Fukushi, K. Solubility of Calcium Carbonate Hemihydrate (CCHH): Where Does CCHH Occur? *Geochem. Persp. Let.* **2024**, *31*, 27–31. [CrossRef]
24. Jiang, J.; Yan, P.; Liu, C.; Sun, T.; Xu, S.; Li, Q. Amorphous Calcium Carbonate (ACC): Structure, Preparation, Stability and Identification. *Adv. Powder Technol.* **2025**, *36*, 104850. [CrossRef]
25. Wang, Q.; Huang, W.; Wang, J.; Long, F.; Fu, Z.; Xie, J.; Zou, Z. Stabilization and Crystallization Mechanism of Amorphous Calcium Carbonate. *J. Colloid Interface Sci.* **2025**, *680*, 24–35. [CrossRef] [PubMed]
26. Marland, G. The Stability of $CaCO_3 \cdot 6H_2O$ (Ikaite). *Geochim. Cosmochim. Acta* **1975**, *39*, 83–91. [CrossRef]
27. Elfil, H.; Roques, H. Prediction of the Limit of the Metastable Zone in the "$CaCO_3$-CO_2-H_2O" System. *AIChE J.* **2004**, *50*, 1908–1916. [CrossRef]
28. Sekkal, W.; Zaoui, A. Nanoscale Analysis of the Morphology and Surface Stability of Calcium Carbonate Polymorphs. *Sci. Rep.* **2013**, *3*, 1587. [CrossRef]
29. Bushuev, Y.G.; Finney, A.R.; Rodger, P.M. Stability and Structure of Hydrated Amorphous Calcium Carbonate. *Cryst. Growth Des.* **2015**, *15*, 5269–5279. [CrossRef]
30. Guo, D.; Ou, W.; Ning, F.; Fang, B.; Liang, Y.; Ud Din, S.; Zhang, L. Effects of Hydrophilic and Hydrophobic nano-$CaCO_3$ on Kinetics of Hydrate Formation. *Energy Sci. Eng.* **2022**, *10*, 507–524. [CrossRef]
31. Taylor, M.G.; Simmkiss, K.; Greaves, G.N.; Okazaki, M.; Mann, S. An X-Ray Absorption Spectroscopy Study of the Structure and Transformation of Amorphous Calcium Carbonate from Plant Cystoliths. *Proc. R. Soc. Lond. B* **1993**, *252*, 75–80. [CrossRef]
32. Levi-Kalisman, Y.; Raz, S.; Weiner, S.; Addadi, L.; Sagi, I. Structural Differences Between Biogenic Amorphous Calcium Carbonate Phases Using X-Ray Absorption Spectroscopy. *Adv. Funct. Mater.* **2002**, *12*, 43–48. [CrossRef]

33. DeVol, R.T.; Metzler, R.A.; Kabalah-Amitai, L.; Pokroy, B.; Politi, Y.; Gal, A.; Addadi, L.; Weiner, S.; Fernandez-Martinez, A.; Demichelis, R.; et al. Oxygen Spectroscopy and Polarization-Dependent Imaging Contrast (PIC)-Mapping of Calcium Carbonate Minerals and Biominerals. *J. Phys. Chem. B* **2014**, *118*, 8449–8457. [CrossRef]
34. Endovitskii, A.P.; Minkin, M.B. Current Problems of the Carbonate System in Soil Solution Thermodynamics. *Pochvovedenie* **1986**, *11*, 76–88.
35. Gal, J.; Bollinger, J.; Tolosa, H.; Gache, N. Calcium Carbonate Solubility: A Reappraisal of Scale Formation and Inhibition. *Talanta* **1996**, *43*, 1497–1509. [CrossRef] [PubMed]
36. Marion, G.M.; Millero, F.J.; Feistel, R. Precipitation of Solid Phase Calcium Carbonates and Their Effect on Application of Seawater S_A–*T*–*P* Models. *Ocean Sci.* **2009**, *5*, 285–291. [CrossRef]
37. Geilfus, N.-X.; Carnat, G.; Dieckmann, G.S.; Halden, N.; Nehrke, G.; Papakyriakou, T.; Tison, J.-L.; Delille, B. First Estimates of the Contribution of $CaCO_3$ Precipitation to the Release of CO_2 to the Atmosphere during Young Sea Ice Growth. *JGR Ocean.* **2013**, *118*, 244–255. [CrossRef]
38. Papadimitriou, S.; Kennedy, H.; Kennedy, P.; Thomas, D.N. Kinetics of Ikaite Precipitation and Dissolution in Seawater-Derived Brines at Sub-Zero Temperatures to 265 K. *Geochim. Cosmochim. Acta* **2014**, *140*, 199–211. [CrossRef]
39. Vasileva, K.; Zaretskaya, N.; Ershova, V.; Rogov, M.; Stockli, L.D.; Stockli, D.; Khaitov, V.; Maximov, F.; Chernyshova, I.; Soloshenko, N.; et al. New Model for Seasonal Ikaite Precipitation: Evidence from White Sea Glendonites. *Mar. Geol.* **2022**, *449*, 106820. [CrossRef]
40. Zaoui, A.; Sekkal, W. Mechanisms behind the Ikaite-to-Calcite Phase Transformation from Molecular Dynamics Calculations. *Geoderma* **2014**, *235–236*, 329–333. [CrossRef]
41. Galan, I.; Purgstaller, B.; Grengg, C.; Müller, B.; Dietzel, M. Amorphous and Crystalline $CaCO_3$ Phase Transformation at High Solid/Liquid Ratio—Insight to a Novel Binder System. *J. Cryst. Growth* **2022**, *580*, 126465. [CrossRef]
42. Sun, R.; Willhammar, T.; Svensson Grape, E.; Strømme, M.; Cheung, O. Mesoscale Transformation of Amorphous Calcium Carbonate to Porous Vaterite Microparticles with Morphology Control. *Cryst. Growth Des.* **2019**, *19*, 5075–5087. [CrossRef]
43. Munemoto, T.; Fukushi, K. Transformation Kinetics of Monohydrocalcite to Aragonite in Aqueous Solutions. *J. Mineral. Petrol. Sci.* **2008**, *103*, 345–349. [CrossRef]
44. Sawada, K. The Mechanisms of Crystallization and Transformation of Calcium Carbonates. *Pure Appl. Chem.* **1997**, *69*, 921–928. [CrossRef]
45. Sánchez-Pastor, N.; Oehlerich, M.; Astilleros, J.M.; Kaliwoda, M.; Mayr, C.C.; Fernández-Díaz, L.; Schmahl, W.W. Crystallization of Ikaite and Its Pseudomorphic Transformation into Calcite: Raman Spectroscopy Evidence. *Geochim. Cosmochim. Acta* **2016**, *175*, 271–281. [CrossRef]
46. Lee, S.-W.; Kim, Y.-I.; Lee, K.; Bang, J.-H.; Jun, C.-W.; Jang, Y.-N. Effect of Serine and Arginine on the Phase Transition from Amorphous $CaCO_3$ and $CaCO_3{\cdot}6H_2O$ to Calcite Film. *Mater. Trans.* **2012**, *53*, 1732–1738. [CrossRef]
47. Larsen, D. Origin and Paleoenvironmental Significance of Calcite Pseudomorphs after Ikaite in the Oligocene Creede Formation, Colorado. *J. Sediment. Res.* **1994**, *64*, 593–603. [CrossRef]
48. De Lurio, J.L.; Frakes, L.A. Glendonites as a Paleoenvironmental Tool: Implications for Early Cretaceous High Latitude Climates in Australia. *Geochim. Cosmochim. Acta* **1999**, *63*, 1039–1048. [CrossRef]
49. Huggett, J.M.; Schultz, B.P.; Shearman, D.J.; Smith, A.J. The Petrology of Ikaite Pseudomorphs and Their Diagenesis. *Proc. Geol. Assoc.* **2005**, *116*, 207–220. [CrossRef]
50. Rogov, M.; Ershova, V.; Vereshchagin, O.; Vasileva, K.; Mikhailova, K.; Krylov, A. Database of Global Glendonite and Ikaite Records throughout the Phanerozoic. *Earth Syst. Sci. Data* **2021**, *13*, 343–356. [CrossRef]
51. Rachlin, A.L.; Henderson, G.S.; Goh, M.C. An Atomic Force Microscope (AFM) Study of the Calcite Cleavage Plane: Image Averaging in Fourier Space. *Am. Min.* **1992**, *77*, 904–910.
52. Kwak, M.; Shindo, H. Atomic Force Microscopic Observation of Facet Formation on Various Faces of Aragonite in Aqueous Acetic Acid. *J. Cryst. Growth* **2005**, *275*, e1655–e1659. [CrossRef]
53. Ranawat, Y.S.; Jaques, Y.M.; Foster, A.S. Predicting Hydration Layers on Surfaces Using Deep Learning. *Nanoscale Adv.* **2021**, *3*, 3447–3453. [CrossRef] [PubMed]
54. Albright, J.N. Mineralogical Notes Vaterite Stability. *Am. Mineral.* **1971**, *56*, 620–624.
55. Pelouze, M.J. Sur Une Combinaison Nouvelle d'eau et de Carbonate de Chaux. *Chem. Rev.* **1865**, *60*, 429–431.
56. Pauly, H. "Ikaite", a New Mineral from Greenland. *ARCTIC* **1963**, *16*, 263–264. [CrossRef]
57. Copisarow, M. XCII.—Heteromorphism of Calcium Carbonate. Marble, Synthetic and Metamorphic. *J. Chem. Soc., Trans.* **1923**, *123*, 785–796. [CrossRef]
58. Johnston, J.; Merwin, H.E.; Williamson, E.D. The Several Forms of Calcium Carbonate. *Am. J. Sci.* **1916**, *s4-41*, 473–512. [CrossRef]
59. Iwanoff, L.L. Ein Wasserhaltiges Calcium Carbonat Aussen Umgebungen von Nowo-Alexandria (Guv. Lublin). *Ann. Der Geol. Und Mineral. Der Russl.* **1906**, *8*, 23–25.

60. Bischoff, J.L.; Stine, S.; Rosenbauer, R.J.; Fitzpatrick, J.A.; Stafford, T.W. Ikaite Precipitation by Mixing of Shoreline Springs and Lake Water, Mono Lake, California, USA. *Geochim. Cosmochim. Acta* **1993**, *57*, 3855–3865. [CrossRef]
61. Feurdean, A.; Perşoiu, A.; Pazdur, A.; Onac, B.P. Evaluating the Palaeoecological Potential of Pollen Recovered from Ice in Caves: A Case Study from Scărişoara Ice Cave, Romania. *Rev. Palaeobot. Palynol.* **2011**, *165*, 1–10. [CrossRef]
62. Boch, R.; Dietzel, M.; Reichl, P.; Leis, A.; Baldermann, A.; Mittermayr, F.; Pölt, P. Rapid Ikaite ($CaCO_3 \cdot 6H_2O$) Crystallization in a Man-Made River Bed: Hydrogeochemical Monitoring of a Rarely Documented Mineral Formation. *Appl. Geochem.* **2015**, *63*, 366–379. [CrossRef]
63. Mikkelsen, A.; Andersen, A.B.; Engelsen, S.B.; Hansen, H.C.B.; Larsen, O.; Skibsted, L.H. Presence and Dehydration of Ikaite, Calcium Carbonate Hexahydrate, in Frozen Shrimp Shell. *J. Agric. Food Chem.* **1999**, *47*, 911–917. [CrossRef]
64. Swainson, I.P.; Hammond, R.P. Ikaite, $CaCO_3 \cdot 6H_2O$: Cold Comfort for Glendonites as Paleothermometers. *Am. Mineral.* **2001**, *86*, 1530–1533. [CrossRef]
65. Rickaby, R.E.M.; Shaw, S.; Bennitt, G.; Kennedy, H.; Zabel, M.; Lennie, A. Potential of Ikaite to Record the Evolution of Oceanic δ18O. *Geol* **2006**, *34*, 497. [CrossRef]
66. Garvie, L.A.J. Seasonal Formation of Ikaite in Slime Flux Jelly on an Infected Tree (*Populus fremontii*) Wound from the Sonoran Desert. *Sci. Nat.* **2022**, *109*, 48. [CrossRef] [PubMed]
67. Tansman, G.F.; Kindstedt, P.S.; Hughes, J.M. Crystallization and Demineralization Phenomena in Washed-Rind Cheese. *J. Dairy Sci.* **2017**, *100*, 8694–8704. [CrossRef]
68. Bastianini, L.; Rogerson, M.; Brasier, A.; Prior, T.J.; Hardman, K.; Dempsey, E.; Bird, A.; Mayes, W.M. Ikaite Formation in Streams Affected by Steel Waste Leachate: First Report and Potential Impact on Contaminant Dynamics. *Chem. Geol.* **2024**, *644*, 121842. [CrossRef]
69. Tollefsen, E.; Balic-Zunic, T.; Mörth, C.-M.; Brüchert, V.; Lee, C.C.; Skelton, A. Ikaite Nucleation at 35 °C Challenges the Use of Glendonite as a Paleotemperature Indicator. *Sci. Rep.* **2020**, *10*, 8141. [CrossRef] [PubMed]
70. Németh, P.; Töchterle, P.; Dublyansky, Y.; Stalder, R.; Molnár, Z.; Klébert, S.; Spötl, C. Tracing Structural Relicts of the Ikaite-to-Calcite Transformation in Cryogenic Cave Glendonite. *Am. Min.* **2022**, *107*, 1960–1967. [CrossRef]
71. Schultz, B.; Thibault, N.; Huggett, J. The Minerals Ikaite and Its Pseudomorph Glendonite: Historical Perspective and Legacies of Douglas Shearman and Alec K. *Smith. Proc. Geol. Assoc.* **2022**, *133*, 176–192. [CrossRef]
72. Lázár, A.; Demény, A.; Hegyi, I.; Aradi, L.E.; Garvie, L.A.J.; Németh, P. Oxygen Isotopic Re-Equilibration during Transformation of Ikaite to Calcite via Amorphous Calcium Carbonate. *Chem. Geol.* **2025**, *693*, 122980. [CrossRef]
73. Hu, Y.-B.; Wolf-Gladrow, D.A.; Dieckmann, G.S.; Völker, C.; Nehrke, G. A Laboratory Study of Ikaite ($CaCO_3 \cdot 6H_2O$) Precipitation as a Function of pH, Salinity, Temperature and Phosphate Concentration. *Mar. Chem.* **2014**, *162*, 10–18. [CrossRef]
74. Kimura, T.; Koga, N. Monohydrocalcite in Comparison with Hydrated Amorphous Calcium Carbonate: Precipitation Condition and Thermal Behavior. *Cryst. Growth Des.* **2011**, *11*, 3877–3884. [CrossRef]
75. Brooks, R.; Clark, L.M.; Thurston, E.F. Calcium Carbonate and Its Hydrates. *Phil. Trans. R. Soc. Lond. A* **1950**, *243*, 145–167. [CrossRef]
76. Van Tassel, R. Carbonatniederschläge Aus Gemischten Calcium-Magnesiumchloridlösungen. *Z. Anorg. Allg. Chem.* **1962**, *319*, 107–112. [CrossRef]
77. Sapozhnikov, D.G.; Zvetkov, A.I. Precipitation of Hydrous Calcium Carbonate on the Bottom of Lake Issyk-Kul. *Dokl. Akad. Nauk SSSR* **1959**, *124*, 402–404.
78. Carlström, D. A Crystallographic Study of Vertebrate Otoliths. *Biol. Bull.* **1963**, *125*, 441–463. [CrossRef]
79. Dahl, K.; Buchardt, B. Monohydrocalcite in the Arctic Ikka Fjord, SW Greenland: First Reported Marine Occurrence. *J. Sediment. Res.* **2006**, *76*, 460–471. [CrossRef]
80. Marschner, H. Hydrocalcite ($CaCO_3 \cdot H_2O$) and Nesquehonite ($MgCO_3 \cdot 3H_2O$) in Carbonate Scales. *Science* **1969**, *165*, 1119–1121. [CrossRef] [PubMed]
81. Garvie, L.A.J. Decay-Induced Biomineralization of the Saguaro Cactus (*Carnegiea gigantea*). *Am. Min.* **2003**, *88*, 1879–1888. [CrossRef]
82. Zaytseva, L.V.; Samylina, O.S.; Prokin, A.A. Formation of Monohydrocalcite in the Microbialites from Laguna de Los Cisnes (Isla Grande de Tierra Del Fuego, Chile). *Environ. Sci. Proc.* **2021**, *6*, 2.
83. Krauss, F.; Schriever, W. Die Hydrate Des Calciumcarbonats. *Z. Anorg. Allg. Chem.* **1930**, *188*, 259–273. [CrossRef]
84. Duedall, I.W.; Buckley, D.E. Calcium Carbonate Monohydrate in Seawater. *Nat. Phys. Sci.* **1971**, *234*, 39–40. [CrossRef]
85. Nathan, C.C. Vaterite in Lake Water. *Nat. Phys. Sci.* **1971**, *231*, 158. [CrossRef]
86. Vereshchagin, O.S.; Chernyshova, I.A.; Kuz'mina, M.A.; Frank-Kamenetskaya, O.V. Calcium Carbonate Precipitation Behavior in the System Ca-Me^{2+}-CO_3-H_2O (Me^{2+} = Co, Ni, Cu, Fe): Ion Incorporation, Effect of Temperature and Aging. *Minerals* **2023**, *13*, 1497. [CrossRef]
87. Rodriguez-Blanco, J.D.; Shaw, S.; Bots, P.; Roncal-Herrero, T.; Benning, L.G. The Role of Mg in the Crystallization of Monohydrocalcite. *Geochim. Cosmochim. Acta* **2014**, *127*, 204–220. [CrossRef]

88. Kitajima, T.; Fukushi, K.; Yoda, M.; Takeichi, Y.; Takahashi, Y. Simple, Reproducible Synthesis of Pure Monohydrocalcite with Low Mg Content. *Minerals* **2020**, *10*, 346. [CrossRef]
89. Zhang, G.; Delgado-López, J.M.; Choquesillo-Lazarte, D.; García-Ruiz, J.M. Growth Behavior of Monohydrocalcite ($CaCO_3 \cdot H_2O$) in Silica-Rich Alkaline Solution. *Cryst. Growth Des.* **2015**, *15*, 564–572. [CrossRef]
90. Kralj, D.; Brečević, L. Dissolution Kinetics and Solubility of Calcium Carbonate Monohydrate. *Colloids Surf. A Physicochem. Eng. Asp.* **1995**, *96*, 287–293. [CrossRef]
91. Taylor, G.F. The Occurrence of Monohydrocalcite in Two Small Lakes in the South-East of South Australia. *Am. Mineral.* **1975**, *60*, 690–697.
92. Zhou, Y.; Liu, Q.; Hu, M.; Xu, G.; Xu, R.; Chong, X.; Feng, J. Investigation on the Stability, Electronic, Optical, and Mechanical Properties of Novel Calcium Carbonate Hydrates via First-principles Calculations. *Int. J. Quantum Chem.* **2020**, *120*, e26219. [CrossRef]
93. Minchin, E.A. "Sponge-Spicules." A Summary of Present Knowledge. *Ergeb. Fortschr. Zool.* **1909**, *2*, 171–274.
94. Kendall, J. XCVI. The Solubility of Calcium Carbonate in Water. *Lond. Edinb. Dubl. Phil. Mag.* **1912**, *23*, 958–976. [CrossRef]
95. Dorfmüller, G. Deut. *Zuckerind* **1938**, *51*, 1217.
96. Schmidt, W.J. *Die Bausteine Des Tierkörpers in Polarisiertem Lieht*; Cohen: Bonn, Germany, 1924; pp. 528–529.
97. Prenant, M. Les Formes Minéralogiques Du Calcaire Chez Les Êtres Vivants, et Le Problème de Leur Déterminisme. *Biol. Rev.* **1927**, *2*, 365–393. [CrossRef]
98. Rinne, F. Quoted in a Footnote by Prenant, M. *Bull. Biol. Fr. Belg.* **1928**, *62*, 21.
99. Odum, H.T. Nudibranch Spicules Made of Amorphous Calcium Carbonate. *Science* **1951**, *114*, 395. [CrossRef]
100. Towe, K.M.; Malone, P.G. Precipitation of Metastable Carbonate Phases from Seawater. *Nature* **1970**, *226*, 348–349. [CrossRef]
101. Enyedi, N.T.; Makk, J.; Kótai, L.; Berényi, B.; Klébert, S.; Sebestyén, Z.; Molnár, Z.; Borsodi, A.K.; Leél-Őssy, S.; Demény, A.; et al. Cave Bacteria-Induced Amorphous Calcium Carbonate Formation. *Sci. Rep.* **2020**, *10*, 8696. [CrossRef]
102. Garvie, L.A.J.; Németh, P.; Trif, L. An Exceptionally Stable and Widespread Hydrated Amorphous Calcium Carbonate Precipitated by the Dog Vomit Slime Mold *Fuligo septica* (Myxogastria). *Sci Rep* **2022**, *12*, 3642. [CrossRef]
103. Gago-Duport, L.; Briones, M.J.I.; Rodríguez, J.B.; Covelo, B. Amorphous Calcium Carbonate Biomineralization in the Earthworm's Calciferous Gland: Pathways to the Formation of Crystalline Phases. *J. Struct. Biol.* **2008**, *162*, 422–435. [CrossRef]
104. Marxen, J.C.; Becker, W.; Finke, D.; Hasse, B.; Epple, M. Early Mineralization in Biomphalaria Glabrata: Microscopic and Structural Results. *J. Molluscan Stud.* **2003**, *69*, 113–121. [CrossRef]
105. Ito, T. Factors Controlling the Transformation of Natural Ikaite from Shiowakka, Japan. *Geochem. J.* **1998**, *32*, 267–273. [CrossRef]
106. Weiner, S.; Levi-Kalisman, Y.; Raz, S.; Addadi, L. Biologically Formed Amorphous Calcium Carbonate. *Connect. Tissue Res.* **2003**, *44*, 214–218. [CrossRef]
107. Meldrum, F.C. Calcium Carbonate in Biomineralisation and Biomimetic Chemistry. *Int. Mater. Rev.* **2003**, *48*, 187–224. [CrossRef]
108. Faatz, M.; Gröhn, F.; Wegner, G. Amorphous Calcium Carbonate: Synthesis and Potential Intermediate in Biomineralization. *Adv. Mater.* **2004**, *16*, 996–1000. [CrossRef]
109. Addadi, L.; Raz, S.; Weiner, S. Taking Advantage of Disorder: Amorphous Calcium Carbonate and Its Roles in Biomineralization. *Adv. Mater.* **2003**, *15*, 959–970. [CrossRef]
110. Addadi, L.; Joester, D.; Nudelman, F.; Weiner, S. Mollusk Shell Formation: A Source of New Concepts for Understanding Biomineralization Processes. *Chem.-Eur. J.* **2006**, *12*, 980–987. [CrossRef]
111. Lam, R.S.K.; Charnock, J.M.; Lennie, A.; Meldrum, F.C. Synthesis-Dependant Structural Variations in Amorphous Calcium Carbonate. *CrystEngComm* **2007**, *9*, 1226–1236. [CrossRef]
112. Xiao, J.; Yang, S. Bio-Inspired Synthesis: Understanding and Exploitation of the Crystallization Process from Amorphous Precursors. *Nanoscale* **2012**, *4*, 54–65. [CrossRef]
113. Feng, Q. Müller, W.E.G., Ed.; Principles of Calcium-Based Biomineralization. In *Molecular Biomineralization*; Progress in Molecular and Subcellular Biology; Springer: Berlin/Heidelberg, Germany, 2011; Volume 52, pp. 141–197, ISBN 978-3-642-21229-1.
114. Lippmann, F. *Sedimentary Carbonate Minerals*; Minerals, Rocks and Mountains Ser; Springer: Berlin/Heidelberg, Germany, 1973; ISBN 978-3-642-65474-9.
115. Deng, S.; Dong, H.; Lv, G.; Jiang, H.; Yu, B.; Bishop, M.E. Microbial Dolomite Precipitation Using Sulfate Reducing and Halophilic Bacteria: Results from Qinghai Lake, Tibetan Plateau, NW China. *Chem. Geol.* **2010**, *278*, 151–159. [CrossRef]
116. Pósfai, M.; Axisa, D.; Tompa, É.; Freney, E.; Bruintjes, R.; Buseck, P.R. Interactions of Mineral Dust with Pollution and Clouds: An Individual-Particle TEM Study of Atmospheric Aerosol from Saudi Arabia. *Atmos. Res.* **2013**, *122*, 347–361. [CrossRef]
117. Ma, G.; He, X.; Jiang, X.; Liu, H.; Chu, J.; Xiao, Y. Strength and Permeability of Bentonite-Assisted Biocemented Coarse Sand. *Can. Geotech. J.* **2021**, *58*, 969–981. [CrossRef]
118. Rostási, Á.; Rácz, K.; Fodor, M.A.; Topa, B.; Molnár, Z.; Weiszburg, T.G.; Pósfai, M. Pathways of Carbonate Sediment Accumulation in a Large, Shallow Lake. *Front. Earth Sci.* **2022**, *10*, 1067105. [CrossRef]

119. Molnár, Z.; Dódony, I.; Pósfai, M. Transformation of Amorphous Calcium Carbonate in the Presence of Magnesium, Phosphate, and Mineral Surfaces. *Geochim. Cosmochim. Acta* **2023**, *345*, 90–101. [CrossRef]
120. Larsen, D.; Crossey, L.J. Depositional Environments and Paleolimnology of an Ancient Caldera Lake: Oligocene Creede Formation, Colorado. *Geol. Soc. America. Bull.* **1996**, *108*, 526. [CrossRef]
121. Dempster, T.; Jess, S.A. Ikaite Pseudomorphs in Neoproterozoic Dalradian Slates Record Earth's Coldest Metamorphism. *J. Geol. Soc.* **2015**, *172*, 459–464. [CrossRef]
122. Vickers, M.L.; Price, G.D.; Jerrett, R.M.; Sutton, P.; Watkinson, M.P.; FitzPatrick, M. The Duration and Magnitude of Cretaceous Cool Events: Evidence from the Northern High Latitudes. *Geol. Soc. Am. Bull.* **2019**, *131*, 1979–1994. [CrossRef]
123. Vasileva, K.; Rogov, M.; Ershova, V.; Mikhailova, K.; Vereshchagin, O.; Pokrovsky, B. Ikaite versus Seep-Related Carbonate Precipitation in the Late Jurassic–Early Cretaceous of West Spitsbergen: Evidence for Cold versus Warm Climates? *Int. J. Earth. Sci. (Geol. Rundsch.)* **2024**, *113*, 417–439. [CrossRef]
124. Zhao, Y.; Yuan, J.; Zhang, J.; Xie, L.; Ji, Z.; Su, M.; Chen, J. A Different Approach for Seawater Decalcification Pretreatment Using Carbon Dioxide as Precipitator. *Desalination* **2013**, *322*, 151–158. [CrossRef]
125. Vassilev, S.V.; Vassileva, C.G.; Petrova, N.L. Mineral Carbonation of Biomass Ashes in Relation to Their CO_2 Capture and Storage Potential. *ACS Omega* **2021**, *6*, 14598–14611. [CrossRef]
126. Gomez-Villalba, L.S.; Feijoo, J.; Rabanal, M.E.; Fort, R. In-Situ Electrochemical Synthesis of Inorganic Compounds for Materials Conservation: Assessment of Their Effects on the Porous Structure. *Ceram. Int.* **2021**, *47*, 30406–30424. [CrossRef]
127. Jones, E.M.; Bakker, D.C.E.; Venables, H.J.; Whitehouse, M.J.; Korb, R.E.; Watson, A.J. Rapid Changes in Surface Water Carbonate Chemistry during Antarctic Sea Ice Melt. *Tellus B: Chem. Phys. Meteorol.* **2010**, *62*, 621–635. [CrossRef]
128. Mortenson, E.; Steiner, N.; Monahan, A.H.; Miller, L.A.; Geilfus, N.-X.; Brown, K. A Model-Based Analysis of Physical and Biogeochemical Controls on Carbon Exchange in the Upper Water Column, Sea Ice, and Atmosphere in a Seasonally Ice-Covered Arctic Strait. *J. Geophys. Res. Ocean.* **2018**, *123*, 7529–7549. [CrossRef]
129. Skelton, A.; Tollefsen, E. Methode for Preparation of Ikaite Crystals and for Carbon Capture and Storage. 2021. Available online: https://worldwide.espacenet.com/patent/search/family/077745389/publication/SE543928C2?q=SE543928C2 (accessed on 21 September 2025).
130. Liu, H.; Wen, Z.; Liu, Z.; Yang, Y.; Wang, H.; Xia, X.; Ye, J.; Liu, Y. Unlocking the Potential of Amorphous Calcium Carbonate: A Star Ascending in the Realm of Biomedical Application. *Acta Pharm. Sin. B.* **2024**, *14*, 602–622. [CrossRef]
131. Konrad, F.; Gallien, F.; Gerard, D.E.; Dietzel, M. Transformation of Amorphous Calcium Carbonate in Air. *Cryst. Growth Des.* **2016**, *16*, 6310–6317. [CrossRef]
132. Du, H.; Steinacher, M.; Borca, C.; Huthwelker, T.; Murello, A.; Stellacci, F.; Amstad, E. Amorphous $CaCO_3$: Influence of the Formation Time on Its Degree of Hydration and Stability. *J. Am. Chem. Soc.* **2018**, *140*, 14289–14299. [CrossRef]
133. Xto, J.M.; Borca, C.N.; Van Bokhoven, J.A.; Huthwelker, T. Aerosol-Based Synthesis of Pure and Stable Amorphous Calcium Carbonate. *Chem. Commun.* **2019**, *55*, 10725–10728. [CrossRef] [PubMed]
134. Chen, S.-F.; Cölfen, H.; Antonietti, M.; Yu, S.-H. Ethanol Assisted Synthesis of Pure and Stable Amorphous Calcium Carbonate Nanoparticles. *Chem. Commun.* **2013**, *49*, 9564–9566. [CrossRef]
135. Zou, Z.; Bertinetti, L.; Habraken, W.J.E.M.; Fratzl, P. Reentrant Phase Transformation from Crystalline Ikaite to Amorphous Calcium Carbonate. *CrystEngComm* **2018**, *20*, 2902–2906. [CrossRef]
136. Coleyshaw, E.E.; Crump, G.; Griffith, W.P. Vibrational Spectra of the Hydrated Carbonate Minerals Ikaite, Monohydrocalcite, Lansfordite and Nesquehonite. *Spectrochim. Acta-A Mol. Biomol. Spectrosc.* **2003**, *59*, 2231–2239. [CrossRef]
137. Aufort, J.; Demichelis, R. Magnesium Impurities Decide the Structure of Calcium Carbonate Hemihydrate. *Cryst. Growth Des.* **2020**, *20*, 8028–8038. [CrossRef]
138. Avaro, J.T.; Ruiz-Agudo, C.; Landwehr, E.; Hauser, K.; Gebauer, D. Impurity-Free Amorphous Calcium Carbonate, a Preferential Material for Pharmaceutical and Medical Applications. *Eur. J. Mineral.* **2019**, *31*, 231–236. [CrossRef]
139. Tlili, M.M.; Amor, M.B.; Gabrielli, C.; Joiret, S.; Maurin, G.; Rousseau, P. Characterization of $CaCO_3$ Hydrates by micro-Raman Spectroscopy. *J. Raman Spectrosc.* **2002**, *33*, 10–16. [CrossRef]
140. Effenberger, H. Kristallstruktur und Infrarot-Absorptionsspektrum von synthetischem Monohydrocalcit, $CaCO_3 \cdot H_2O$. *Monatsh. Fur Chem.* **1981**, *112*, 899–909. [CrossRef]
141. Korneva, T.A.; Kovaleva, L.T.; Lyubushko, G.I. Thermal Analysis and IR-Spectroscopic Study of Synthetic Hydrocalcite. *Term. An. I Faz. Ravnovesiya Perm* **1983**, *43*, 94–97.
142. Dickens, B.; Brown, W.E. Crystal Structure of Calcium Carbonate Hexahydrate at about −120°. *Inorg. Chem.* **1970**, *9*, 480–486. [CrossRef]
143. Hesse, K.-F.; Küppers, H.; Suess, E. Refinement of the Structure of Ikaite, $CaCO_3 \cdot 6H_2O$. *Z. Für Krist.-Cryst. Mater.* **1983**, *163*, 227–231. [CrossRef]
144. Lennie, A.R.; Tang, C.C.; Thompson, S.P. The Structure and Thermal Expansion Behaviour of Ikaite, $CaCO_3 \cdot 6H_2O$, from T = 114 to T = 293 K. *Mineral. Mag.* **2004**, *68*, 135–146. [CrossRef]

145. Tateno, N.; Kyono, A. Structural Change Induced by Dehydration in Ikaite ($CaCO_3 \cdot 6H_2O$). *J. Min. Petr. Econ. Geol.* **2014**, *109*, 157–168. [CrossRef]
146. Chahi, G.; Bradai, D.; Belabbas, I. Structural and Elastic Properties of $CaCO_3$ Hydrated Phases: A Dispersion-Corrected Density Functional Theory Study. *J. Phys. Chem. Solids* **2020**, *138*, 109295. [CrossRef]
147. Singer, J.W.; Yazaydin, A.Ö.; Kirkpatrick, R.J.; Bowers, G.M. Structure and Transformation of Amorphous Calcium Carbonate: A Solid-State^{43} Ca NMR and Computational Molecular Dynamics Investigation. *Chem. Mater.* **2012**, *24*, 1828–1836. [CrossRef]
148. Costa, S.N.; Freire, V.N.; Caetano, E.W.S.; Maia, F.F.; Barboza, C.A.; Fulco, U.L.; Albuquerque, E.L. DFT Calculations with van Der Waals Interactions of Hydrated Calcium Carbonate Crystals $CaCO_3 \cdot (H_2O, 6H_2O)$: Structural, Electronic, Optical, and Vibrational Properties. *J. Phys. Chem. A* **2016**, *120*, 5752–5765. [CrossRef]
149. Swainson, I.P. The Structure of Monohydrocalcite and the Phase Composition of the Beachrock Deposits of Lake Butler and Lake Fellmongery, South Australia. *Am. Mineral.* **2008**, *93*, 1014–1018. [CrossRef]
150. Mincheva-Stefanova, Y.; Neikov, K. Trigonal-Trapezohedral Monohydrocalcite from an Oxidation Zone. *Dokl. Bulg. Acad. Nauk.* **1990**, *43*, 57–60.
151. Makovicky, E. The Order–Disorder Potential of the Crystal Structure of Monohydrocalcite, $CaCO_3 \cdot H_2O$. *Miner. Petrol.* **2018**, *112*, 105–109. [CrossRef]
152. Demichelis, R.; Raiteri, P.; Gale, J.D.; Dovesi, R. Examining the Accuracy of Density Functional Theory for Predicting the Thermodynamics of Water Incorporation into Minerals: The Hydrates of Calcium Carbonate. *J. Phys. Chem. C* **2013**, *117*, 17814–17823. [CrossRef]
153. Demichelis, R.; Raiteri, P.; Gale, J.D. Structure of Hydrated Calcium Carbonates: A First-Principles Study. *J. Cryst. Growth* **2014**, *401*, 33–37. [CrossRef]
154. Michel, F.M.; MacDonald, J.; Feng, J.; Phillips, B.L.; Ehm, L.; Tarabrella, C.; Parise, J.B.; Reeder, R.J. Structural Characteristics of Synthetic Amorphous Calcium Carbonate. *Chem. Mater.* **2008**, *20*, 4720–4728. [CrossRef]
155. Quigley, D.; Rodger, P.M. Free Energy and Structure of Calcium Carbonate Nanoparticles during Early Stages of Crystallization. *J. Chem. Phys.* **2008**, *128*, 221101. [CrossRef] [PubMed]
156. Raiteri, P.; Gale, J.D. Water Is the Key to Nonclassical Nucleation of Amorphous Calcium Carbonate. *J. Am. Chem. Soc.* **2010**, *132*, 17623–17634. [CrossRef]
157. Goodwin, A.L.; Michel, F.M.; Phillips, B.L.; Keen, D.A.; Dove, M.T.; Reeder, R.J. Nanoporous Structure and Medium-Range Order in Synthetic Amorphous Calcium Carbonate. *Chem. Mater.* **2010**, *22*, 3197–3205. [CrossRef]
158. Quigley, D.; Freeman, C.L.; Harding, J.H.; Rodger, P.M. Sampling the Structure of Calcium Carbonate Nanoparticles with Metadynamics. *J. Chem. Phys.* **2011**, *134*, 044703. [CrossRef] [PubMed]
159. Saharay, M.; James Kirkpatrick, R. Onset of Orientational Order in Amorphous Calcium Carbonate (ACC) upon Dehydration. *Chem. Phys. Lett.* **2014**, *591*, 287–291. [CrossRef]
160. Lopez-Berganza, J.A.; Diao, Y.; Pamidighantam, S.; Espinosa-Marzal, R.M. Ab Initio Studies of Calcium Carbonate Hydration. *J. Phys. Chem. A* **2015**, *119*, 11591–11600. [CrossRef]
161. Innocenti Malini, R.; Bushuev, Y.G.; Hall, S.A.; Freeman, C.L.; Rodger, P.M.; Harding, J.H. Using Simulation to Understand the Structure and Properties of Hydrated Amorphous Calcium Carbonate. *CrystEngComm* **2016**, *18*, 92–101. [CrossRef]
162. Saharuddin, T.S.T.; Samsuri, A.; Salleh, F.; Othaman, R.; Kassim, M.B.; Mohamed Hisham, M.W.; Yarmo, M.A. Studies on Reduction of Chromium Doped Iron Oxide Catalyst Using Hydrogen and Various Concentration of Carbon Monoxide. *Int. J. Hydrogen Energy* **2017**, *42*, 9077–9086. [CrossRef]
163. Jensen, A.C.S.; Imberti, S.; Habraken, W.J.E.M.; Bertinetti, L. Small Ionic Radius Limits Magnesium Water Interaction in Amorphous Calcium/Magnesium Carbonates. *J. Phys. Chem. C* **2020**, *124*, 6141–6144. [CrossRef]
164. Schmidt, M.P.; Ilott, A.J.; Phillips, B.L.; Reeder, R.J. Structural Changes upon Dehydration of Amorphous Calcium Carbonate. *Cryst. Growth Des.* **2014**, *14*, 938–951. [CrossRef]
165. Jensen, A.C.S.; Imberti, S.; Parker, S.F.; Schneck, E.; Politi, Y.; Fratzl, P.; Bertinetti, L.; Habraken, W.J.E.M. Hydrogen Bonding in Amorphous Calcium Carbonate and Molecular Reorientation Induced by Dehydration. *J. Phys. Chem. C* **2018**, *122*, 3591–3598. [CrossRef]
166. Sand, K.K.; Rodriguez-Blanco, J.D.; Makovicky, E.; Benning, L.G.; Stipp, S.L.S. Crystallization of $CaCO_3$ in Water–Alcohol Mixtures: Spherulitic Growth, Polymorph Stabilization, and Morphology Change. *Cryst. Growth Des.* **2012**, *12*, 842–853. [CrossRef]
167. Besselink, R.; Rodriguez-Blanco, J.D.; Stawski, T.M.; Benning, L.G.; Tobler, D.J. How Short-Lived Ikaite Affects Calcite Crystallization. *Cryst. Growth Des.* **2017**, *17*, 6224–6230. [CrossRef]
168. Van Driessche, A.E.S.; Kellermeier, M.; Benning, L.G.; Gebauer, D. (Eds.) *New Perspectives on Mineral Nucleation and Growth*; Springer International Publishing: Cham, Switzerland, 2017; ISBN 978-3-319-45667-6.
169. Huang, Y.; Rao, A.; Huang, S.; Chang, C.; Drechsler, M.; Knaus, J.; Chan, J.C.C.; Raiteri, P.; Gale, J.D.; Gebauer, D. Uncovering the Role of Bicarbonate in Calcium Carbonate Formation at Near-Neutral pH. *Angew. Chem. Int. Ed.* **2021**, *60*, 16707–16713. [CrossRef]

170. Wang, Q.; Zou, Z.; Wang, H.; Wang, W.; Fu, Z. Pressure-Induced Crystallization and Densification of Amorphized Calcium Carbonate Hexahydrate Controlled by Interfacial Water. *J. Colloid Interface Sci.* **2022**, *611*, 346–355. [CrossRef]
171. Katsikopoulos, D.; Fernández-González, Á.; Prieto, A.C.; Prieto, M. Co-Crystallization of Co(II) with Calcite: Implications for the Mobility of Cobalt in Aqueous Environments. *Chem. Geol.* **2008**, *254*, 87–100. [CrossRef]
172. Shuseki, Y.; Kohara, S.; Ohara, K.; Ohkubo, T.; Takei, K.; Tucker, M.G.; Kolesnikov, A.I.; Mcdonnell, M.T.; Sacci, R.L.; Neuefeind, J.C.; et al. Structural Analyses of Amorphous Calcium Carbonate before and after Removing Strontium Ions from an Aqueous Solution. *J. Ceram. Soc. Jpn.* **2022**, *130*, 225–231. [CrossRef]
173. Molnár, Z.; Hegedűs, M.; Németh, P.; Pósfai, M. Competitive Incorporation of Ca, Sr, and Ba Ions into Amorphous Carbonates. *Geochim. Cosmochim. Acta* **2025**, *393*, 18–30. [CrossRef]
174. Roberts, N.M.W.; Holdsworth, R.E. Timescales of Faulting through Calcite Geochronology: A Review. *J. Struct. Geol.* **2022**, *158*, 104578. [CrossRef]
175. Fyfe, W.S.; Bischoff, J.L. The Calcite-Aragonite Problem[1]. In *Dolomitization and Limestone Diagenesis*; SEPM Society for Sedimentary Geology: Claremore, OK, USA, 1965; ISBN 978-1-56576-143-8.
176. Zhao, S.; Schettino, E.; Merlini, M.; Poli, S. The Stability and Melting of Aragonite: An Experimental and Thermodynamic Model for Carbonated Eclogites in the Mantle. *Lithos* **2019**, *324–325*, 105–114. [CrossRef]
177. Cooke, R.C.; Kepkay, P.E. The Solubility of Aragonite in Seawater—I. Effect of pH and Water Chemistry at One Atmosphere. *Geochim. Cosmochim. Acta* **1980**, *44*, 1071–1075. [CrossRef]
178. Spanos, N.; Koutsoukos, P.G. The Transformation of Vaterite to Calcite: Effect of the Conditions of the Solutions in Contact with the Mineral Phase. *J. Cryst. Growth* **1998**, *191*, 783–790. [CrossRef]
179. Vereshchagin, O.S.; Frank-Kamenetskaya, O.V.; Kuz'mina, M.A.; Chernyshova, I.A.; Shilovskikh, V.V. Effect of Magnesium on Monohydrocalcite Formation and Unit-Cell Parameters. *Am. Mineral.* **2021**, *106*, 1294–1305. [CrossRef]
180. Rodriguez-Blanco, J.D.; Shaw, S.; Benning, L.G. The Kinetics and Mechanisms of Amorphous Calcium Carbonate (ACC) Crystallization to Calcite, Viavaterite. *Nanoscale* **2011**, *3*, 265–271. [CrossRef]
181. Lennie, A.R. Ikaite ($CaCO_3 \cdot 6H_2O$) Compressibility at High Water Pressure: A Synchrotron X-Ray Diffraction Study. *Mineral. mag.* **2005**, *69*, 325–335. [CrossRef]
182. Shahar, A. The Stability and Raman Spectra of Ikaite, $CaCO_3 \cdot 6H_2O$, at High Pressure and Temperature. *Am. Mineral.* **2005**, *90*, 1835–1839. [CrossRef]
183. Hu, Y.; Dieckmann, G.S.; Wolf-Gladrow, D.A.; Nehrke, G. Laboratory Study on Coprecipitation of Phosphate with Ikaite in Sea Ice. *J. Geophys. Res. Ocean.* **2014**, *119*, 7007–7015. [CrossRef]
184. Purgstaller, B.; Dietzel, M.; Baldermann, A.; Mavromatis, V. Control of Temperature and Aqueous Mg^{2+}/Ca^{2+} Ratio on the (Trans-)Formation of Ikaite. *Geochim. Cosmochim. Acta* **2017**, *217*, 128–143. [CrossRef]
185. Strohm, S.B.; Saldi, G.D.; Mavromatis, V.; Schmahl, W.W.; Jordan, G. A Study on Ikaite Growth in the Presence of Phosphate. *Aquat. Geochem.* **2023**, *29*, 219–233. [CrossRef]
186. Clarkson, J.R.; Price, T.J.; Adams, C.J. Role of Metastable Phases in the Spontaneous Precipitation of Calcium Carbonate. *J. Chem. Soc., Faraday Trans.* **1992**, *88*, 243–249. [CrossRef]
187. Chaka, A.M. Quantifying the Impact of Magnesium on the Stability and Water Binding Energy of Hydrated Calcium Carbonates by Ab Initio Thermodynamics. *J. Phys. Chem. A* **2019**, *123*, 2908–2923. [CrossRef]
188. Tang, C.C.; Thompson, S.P.; Parker, J.E.; Lennie, A.R.; Azough, F.; Kato, K. The Ikaite-to-Vaterite Transformation: New Evidence from Diffraction and Imaging. *J. Appl. Crystallogr.* **2009**, *42*, 225–233. [CrossRef]
189. Shaikh, A.M. A New Crystal Growth Form of Vaterite, $CaCO_3$. *J. Appl. Crystallogr.* **1990**, *23*, 263–265. [CrossRef]
190. Hull, H.; Turnbull, A.G. A Thermochemical Study of Monohydrocalcite. *Geochim. Cosmochim. Acta* **1973**, *37*, 685–694. [CrossRef]
191. Liu, R.; Liu, F.; Zhao, S.; Su, Y.; Wang, D.; Shen, Q. Crystallization and Oriented Attachment of Monohydrocalcite and Its Crystalline Phase Transformation. *CrystEngComm* **2013**, *15*, 509–515. [CrossRef]
192. Nechiporenko, G.O.; Bondarenko, G.P.; Ermilov, V.V. Effect of Certain Factors on the Formation and Stability of Monohydrocalcite in Seawater. *Zap. Vses. Mineral. O-Va.* **1983**, *112*, 94–103.
193. Nishiyama, R.; Munemoto, T.; Fukushi, K. Formation Condition of Monohydrocalcite from $CaCl_2$–$MgCl_2$–Na_2CO_3 Solutions. *Geochim. Cosmochim. Acta* **2013**, *100*, 217–231. [CrossRef]
194. Dalas, E.; Kallitsis, J.; Koutsoukos, P.G. The Crystallization of Calcium Carbonate on Polymeric Substrates. *J. Cryst. Growth* **1988**, *89*, 287–294. [CrossRef]
195. Giannimaras, E.K.; Koutsoukos, P.G. Precipitation of Calcium Carbonate in Aqueous Solutions in the Presence of Oxalate Anions. *Langmuir* **1988**, *4*, 855–861. [CrossRef]
196. Zhang, G.; Delgado-López, J.M.; Choquesillo-Lazarte, D.; García-Ruiz, J.M. Crystallization of Monohydrocalcite in a Silica-Rich Alkaline Solution. *CrystEngComm* **2013**, *15*, 6526–6532. [CrossRef]
197. Mucci, A.; Morse, J.W. The Incorporation of Mg^{2+} and Sr^{2+} into Calcite Overgrowths: Influences of Growth Rate and Solution Composition. *Geochim. Cosmochim. Acta* **1983**, *47*, 217–233. [CrossRef]

198. Chen, T.; Neville, A.; Yuan, M. Assessing the Effect of on Scale Formation–Bulk Precipitation and Surface Deposition. *J. Cryst. Growth* **2005**, *275*, e1341–e1347. [CrossRef]
199. Von Euw, S.; Azaïs, T.; Manichev, V.; Laurent, G.; Pehau-Arnaudet, G.; Rivers, M.; Murali, N.; Kelly, D.J.; Falkowski, P.G. Solid-State Phase Transformation and Self-Assembly of Amorphous Nanoparticles into Higher-Order Mineral Structures. *J. Am. Chem. Soc.* **2020**, *142*, 12811–12825. [CrossRef]
200. Kimura, T.; Koga, N. Thermal Dehydration of Monohydrocalcite: Overall Kinetics and Physico-Geometrical Mechanisms. *J. Phys. Chem. A* **2011**, *115*, 10491–10501. [CrossRef]
201. Zhang, G.; Verdugo-Escamilla, C.; Choquesillo-Lazarte, D.; García-Ruiz, J.M. Thermal Assisted Self-Organization of Calcium Carbonate. *Nat. Commun.* **2018**, *9*, 5221. [CrossRef]
202. Termine, J.D.; Peckauskas, R.A.; Posner, A.S. Calcium Phosphate Formation in Vitro. *Arch. Biochem. Biophys.* **1970**, *140*, 318–325. [CrossRef] [PubMed]
203. Aizenberg, J.; Addadi, L.; Weiner, S.; Lambert, G. Stabilization of Amorphous Calcium Carbonate by Specialized Macromolecules in Biological and Synthetic Precipitates. *Adv. Mater.* **1996**, *8*, 222–226. [CrossRef]
204. Kababya, S.; Gal, A.; Kahil, K.; Weiner, S.; Addadi, L.; Schmidt, A. Phosphate–Water Interplay Tunes Amorphous Calcium Carbonate Metastability: Spontaneous Phase Separation and Crystallization vs. Stabilization Viewed by Solid State NMR. *J. Am. Chem. Soc.* **2015**, *137*, 990–998. [CrossRef]
205. Purgstaller, B.; Goetschl, K.E.; Mavromatis, V.; Dietzel, M. Solubility Investigations in the Amorphous Calcium Magnesium Carbonate System. *CrystEngComm* **2019**, *21*, 155–164. [CrossRef] [PubMed]
206. Maslyk, M.; Mondeshki, M.; Tremel, W. Amorphous Calcium Carbonate Monohydrate Containing a Defect Hydrate Network by Mechanochemical Processing of Mono-Hydrocalcite Using Ethanol as Auxiliary Solvent. *CrystEngComm* **2022**, *24*, 4687–4697. [CrossRef]
207. Kojima, Y.; Kawanobe, A.; Yasue, T.; Arai, Y. Controls of Polymorphism and Morphology of Calcium Carbonate Compounds Formed by Crystallizing Amorphous Calcium Carbonate Hydrate. *J. Ceram. Soc. Jpn.* **1994**, *102*, 1128–1136. [CrossRef]
208. Kojima, Y.; Endo, N.; Yasue, T.; Arai, Y. Morphological Controls of Calcium Carbonate Hexahydrate and Its Dehydrating Substance. *J. Ceram. Soc. Jpn.* **1995**, *103*, 1282–1288. [CrossRef]
209. Gower, L.A.; Tirrell, D.A. Calcium Carbonate Films and Helices Grown in Solutions of Poly(Aspartate). *J. Cryst. Growth* **1998**, *191*, 153–160. [CrossRef]
210. Gower, L.B.; Odom, D.J. Deposition of Calcium Carbonate Films by a Polymer-Induced Liquid-Precursor (PILP) Process. *J. Cryst. Growth* **2000**, *210*, 719–734. [CrossRef]
211. Sun, S.; Chevrier, D.M.; Zhang, P.; Gebauer, D.; Cölfen, H. Distinct Short-Range Order Is Inherent to Small Amorphous Calcium Carbonate Clusters (<2 Nm). *Angew. Chem. Int. Ed.* **2016**, *55*, 12206–12209. [CrossRef]
212. Yasue, T.; Mamiya, A.; Fukushima, T.; Arai, Y. Synthesis and Characteristics of Amorphous Calcium Carbonate in Ethanol. *Gypsum Lime* **1985**, *198*, 245–252. [CrossRef]
213. Ihli, J.; Wong, W.C.; Noel, E.H.; Kim, Y.-Y.; Kulak, A.N.; Christenson, H.K.; Duer, M.J.; Meldrum, F.C. Dehydration and Crystallization of Amorphous Calcium Carbonate in Solution and in Air. *Nat. Commun.* **2014**, *5*, 3169. [CrossRef]
214. Rodriguez-Blanco, J.D.; Shaw, S.; Benning, L.G. How to Make 'Stable' ACC: Protocol and Preliminary Structural Characterization. *Mineral. Mag.* **2008**, *72*, 283–286. [CrossRef]
215. Gebauer, D.; Gunawidjaja, P.N.; Ko, J.Y.P.; Bacsik, Z.; Aziz, B.; Liu, L.; Hu, Y.; Bergström, L.; Tai, C.; Sham, T.; et al. Proto-Calcite and Proto-Vaterite in Amorphous Calcium Carbonates. *Angew. Chem. Int. Ed.* **2010**, *49*, 8889–8891. [CrossRef]
216. Gebauer, D.; Cölfen, H. Prenucleation Clusters and Non-Classical Nucleation. *Nano Today* **2011**, *6*, 564–584. [CrossRef]
217. Bots, P.; Benning, L.G.; Rodriguez-Blanco, J.-D.; Roncal-Herrero, T.; Shaw, S. Mechanistic Insights into the Crystallization of Amorphous Calcium Carbonate (ACC). *Cryst. Growth Des.* **2012**, *12*, 3806–3814. [CrossRef]
218. Cai, H.; Wang, Q.; Zou, Z. Crystallization Pathway of Monohydrocalcite via Amorphous Calcium Carbonate Regulated by Magnesium Ion. *J. Inorg. Mater.* **2024**, *39*, 1275–1282. [CrossRef]

Disclaimer/Publisher's Note: The statements, opinions and data contained in all publications are solely those of the individual author(s) and contributor(s) and not of MDPI and/or the editor(s). MDPI and/or the editor(s) disclaim responsibility for any injury to people or property resulting from any ideas, methods, instructions or products referred to in the content.